1   **Small proteome of the nitrogen-fixing plant symbiont *Sinorhizobium meliloti***

2

3   Lydia Hadjeras[1], Benjamin Heiniger[2*], Sandra Maaß[3*], Robina Scheuer[4*], Rick Gelhausen[5],

4   Saina Azarderakhsh[4], Susanne Barth-Weber[4], Rolf Backofen[5], Dörte Becher[3], Christian H.

5   Ahrens[2,#], Cynthia M. Sharma[1,#], Elena Evguenieva-Hackenberg[3,#]

6

7   [1]Institute of Molecular Infection Biology, University of Würzburg, 97080 Würzburg, Germany

8   [2]Molecular Ecology, Agroscope and SIB Swiss Institute of Bioinformatics, 8046 Zurich,
9   Switzerland

10   [3]Institute of Microbiology, University of Greifswald, 17489 Greifswald, Germany

11   [4]Institute of Microbiology and Molecular Biology, University of Giessen, 35392 Giessen,
12   Germany

13   [5]Bioinformatics Group, Department of Computer Science, University of Freiburg, 79110
14   Freiburg, Germany

15   *: These authors contributed equally to the study

16   # correspondence

17
18
19   **Corresponding authors:**

20
21   Elena Evguenieva-Hackenberg: Elena.Evguenieva-Hackenberg@mikro.bio.uni-
22   giessen.de

23
24   Cynthia M. Sharma: cynthia.sharma@uni-wuerzburg.de

25
26   Christian H. Ahrens: christian.ahrens@agroscope.admin.ch

27
28

29   **Keywords**

32   **ORCID-IDs** L. Hadjeras: 0000-0003-4645-8044; S. Maaß: 0000-0002-6573-1088; R.
33   Gelhausen: 0000-0003-4161-4394; R. Backofen: 0000-0001-8231-3323; D. Becher: 0000-
34   0002-9630-5735; C.M. Sharma: 0000-0002-2321-9705; C.H. Ahrens: 0000-0002-8148-7257;
35   E. Evguenieva-Hackenberg: 0000-0001-7270-3168

ABSTRACT

The soil-dwelling plant symbiont *Sinorhizobium meliloti* is a major model organism of Alphaproteobacteria. Despite numerous detailed OMICS studies, information about small open reading frame (sORF)-encoded proteins (SEPs) is largely missing, because sORFs are poorly annotated, and SEPs are hard to detect experimentally. However, given that SEPs can fulfill important functions, cataloging the full complement of translated sORFs is critical for analyzing their roles in bacterial physiology. Ribosome profiling (Ribo-seq) can detect translated sORFs with high sensitivity, but is not yet routinely applied to bacteria because it must be adapted for each species. Here, we established a Ribo-seq procedure for *S. meliloti* 2011 based on RNase I digestion and detected translation for 60% of the annotated coding sequences during growth in minimal medium. Using ORF prediction tools based on Ribo-seq data, subsequent filtering, and manual curation, the translation of 37 non-annotated sORFs with ≤ 70 amino acids was predicted with high confidence. The Ribo-seq data were supplemented by mass spectrometry (MS) analyses from three sample preparation approaches and two integrated proteogenomic search databases (iPtgxDBs). Searches against a standard and a 20-fold smaller Ribo-seq data-informed custom iPtgxDB confirmed many annotated SEPs and identified 11 additional novel SEPs. Epitope tagging and Western blot analysis confirmed the translation of 15 out of 20 SEPs selected from the translatome map. Overall, by applying MS and Ribo-seq as complementary approaches, the small proteome of *S. meliloti* was substantially expanded by 48 novel SEPs. Several of them are conserved from *Rhizobiaceae* to Bacteria, suggesting important physiological functions.

1 INTRODUCTION

2 Over the last two decades, using next-generation sequencing and high throughput OMICS
3 profiling technologies, the genomes of thousands of bacteria have been assembled, and
4 the transcriptomes and proteomes of many of them have been analyzed under different
5 conditions, with the aim of gaining insights into the genetic and molecular basis of their
6 biology. Despite this wealth of data, information about small open reading frame (sORF)-
7 encoded proteins (SEPs), which are proteins with less than 50 or 100 amino acids (aa), is
8 scarce (Duval and Cossart 2017; Gray et al. 2022; Hemm et al. 2020; Orr et al. 2020; Storz
9 et al. 2014). Recently, the small proteomes of eukaryotes, bacteria, and viruses have been
10 focused on, as a growing number of small proteins have been demonstrated to fulfill
11 important physiological functions, such as in cell division, metabolism, transport, signal
12 transduction, spore formation, cell communication, cellular stress responses, and
13 virulence (Aoyama et al. 2022; Duval and Cossart 2017; Hemm et al. 2020; Melior et al.
14 2020; Khitun and Slavoff 2019; Patraquim et al. 2020; Song et al. 2022; Storz et al. 2014).
15 Therefore, cataloging the full complement of small proteins is critical in achieving a more
16 comprehensive and accurate description of the proteomes of bacterial model organisms
17 and their potential functions.

18 Small protein identification is difficult due to several technical challenges. For instance,
19 SEPs are difficult to detect using SDS-PAGE or mass spectrometry (MS) for various
20 technical reasons (Ahrens et al. 2022; Fijalkowski et al. 2022; Storz et al. 2014).
21 Limitations of standard shotgun proteomics workflows at the sample preparation,
22 protease digestion, liquid chromatography, MS data acquisition, and bioinformatic data
23 analysis steps affect comprehensive MS-based SEP identification (Ahrens et al. 2022;
24 Cassidy et al. 2021). Furthermore, variable length thresholds were used in the genome
25 annotation step to minimize the number of spurious ORF predictions. As a result, sORFs
26 encoding truly expressed small proteins are often missing from genome annotations
27 (Hahn et al. 2016; Storz et al. 2014). Meanwhile, various strategies to achieve extensive
28 proteome coverage of the notoriously under-represented classes of small and membrane
29 proteins (novel small proteins are often membrane associated) have been applied for
30 prokaryotes (Omasits et al. 2013; Wiśniewski 2016; Zhang et al. 2013). Methods to enrich
31 bacterial SEPs in samples are further improved, for example, with the use of small pore-
32 sized solid-phase materials (Bartel et al. 2020; Cassidy et al. 2019; Petruschke et al. 2020),

1 and digestion with alternative/multiple proteases has been performed to increase the
2 number of identified SEPs (Bartel et al. 2020; Kaulich et al. 2021; Petruschke et al. 2021).
3 The obtained mass spectra are usually assigned to peptide or protein sequences by
4 matching the determined fragment ion masses to the predictions derived from a sequence
5 database (DB). Therefore, only peptides with sequences available in the protein search
6 DB can be identified. Consequently, custom protein search DBs that try to capture the
7 entire coding potential of prokaryotic genomes have been proposed, such as integrated
8 proteogenomic search DBs (iPtgxDBs). They integrate and consolidate the differences
9 among existing reference genome annotations, *ab initio* gene predictions, and a modified
10 six-frame translation by considering alternative start sites, thereby enabling the detection
11 of novel proteins, including SEPs (Omasits et al. 2017). Thus, proteogenomic studies that
12 combine results from SEP-optimized MS data searched with iPtgxDBs or other custom
13 search DBs and ribosome profiling (Ribo-seq) have great potential to detect highly
14 comprehensive and accurate compendia of novel small proteins.

15 Ribo-seq has developed into a powerful method to study and annotate translatome
16 globally, including sORFs (Ingolia 2016; Vazquez-Laslop et al. 2022). Compared with MS-
17 based proteomics, Ribo-seq has the advantage of higher sensitivity (Ahrens et al. 2022;
18 Duval and Cossart 2017; Gray et al. 2022; Hemm et al. 2020; Orr et al. 2020; Venturini et
19 al. 2020; Storz et al. 2014). Ribo-seq relies on deep sequencing of approximately 30-nt-
20 long "footprint" regions of the mRNA bound by the ribosome during translation and
21 protected against nuclease digestion. In addition to providing a global picture of actively
22 translated mRNAs in the cell, Ribo-seq also reveals the specific location on the RNA where
23 the ribosome was bound, allowing the mapping of ORFs. For this, cells are lysed under
24 certain conditions, allowing for the "freezing" of ribosomes on mRNAs. mRNA parts that
25 are not protected by the ribosomes are then digested to generate ribosome footprints that
26 are sequenced and mapped to the genome (Ingolia et al. 2009; Ingolia 2016). While Ribo-
27 seq-based detection of translated mRNA works well for eukaryotic cells at a single codon
28 resolution, this method is difficult to utilize for prokaryotes (Glaub et al. 2020;
29 Mohammad et al. 2019; Vazquez-Laslop et al. 2022). Nevertheless, adapting and refining
30 the Ribo-seq method has enabled the detection of many new, translated sORFs and
31 corresponding SEPs not only in *Escherichia coli* but also in several other bacterial species
32 and in halophilic archaea (Gelsinger et al. 2020; Meydan et al. 2019; Mohammad et al.
33 2019; Vazquez-Laslop et al. 2022; Weaver et al. 2019). However, for many bacterial model

1 organisms, Ribo-seq data are still missing, as the protocols typically have to be adapted
2 and optimized for each bacterial organism (Duval and Cossart 2017; Gray et al. 2022;
3 Hemm et al. 2020; Orr et al. 2020; Venturini et al. 2020; Storz et al. 2014).

4 *Sinorhizobium meliloti* is an agriculturally important bacterial species that lives in soil and
5 can fix molecular nitrogen in symbiosis with legume plants (Jones et al. 2007). Due to its
6 versatile lifestyle and ecological relevance, it is a major model organism for studying gene
7 regulation in Alphaproteobacteria. In addition, its relatively close relationship to
8 pathogens of the genus *Brucella* makes *S. meliloti* an attractive model for host–pathogen
9 research (Marlow et al. 2009). Several OMICS datasets are available for *S. meliloti* 2011
10 and its sibling, *S. meliloti* 1021, which is the first sequenced strain of this species (Galibert
11 et al. 2001). These consist of proteomics (Djordjevic 2004; Barra-Bily et al. 2010; Sobrero
12 et al. 2012; Marx et al. 2016) and transcriptomic datasets, including differential RNA-seq
13 that enables the annotation of transcription start sites, 5′ and 3′ UTRs, and novel
14 transcripts (Becker et al. 2004; Schlüter et al. 2013; Sallet et al. 2013). The *S. meliloti* 2011
15 6.7 Mb genome harbors a 3.66 Mb chromosome and two megaplasmids, the 1.35 Mb
16 pSymA and the 1.68 Mb pSymB (Sallet et al. 2013). As a proof of principle, an iPtgxDB
17 created for *S. meliloti* 2011 has allowed the detection of the 14-aa-long leader peptide
18 peTrpL in the proteomic data, in which a function in resistance to multiple antimicrobial
19 compounds can be subsequently established (Melior et al. 2020). However, the
20 identification of additional functional SEPs in *S. meliloti* and related Alphaproteobacteria
21 has been limited by the lack of studies specifically targeting the small proteome and
22 translatome.

23 Here, we developed and then applied Ribo-seq on *S. meliloti* 2011 to map its translatome
24 globally, with a focus on the small proteome (data available at our interactive web-based
25 genome-browser: http://www.bioinf.uni-freiburg.de/ribobase). The use of RNase I in our
26 Ribo-seq showed successful trimming of mRNA regions that were not protected by
27 ribosomes, allowing differentiation between translated and untranslated regions. Besides
28 detecting the translation of annotated sORFs (some of which are available in recent
29 updates of the genome annotation), we also uncovered 37 translated novel, non-
30 annotated sORFs located on different replicons. The translation of several annotated, as
31 well as novel, sORFs was further validated by MS-based proteomics using iPtgxDBs
32 and/or epitope tagging and Western blot analysis, thereby confirming predictions based

1   on Ribo-seq coverage. Eleven novel SEPs were uniquely identified by MS, showing that

2   using both methods when mapping the small proteome is advantageous. Overall, our

3   combined approach provided a set of 48 novel *S. meliloti* sORFs, many of which are

4   conserved, as a resource to further elucidate their roles in bacterial physiology and

5   symbiosis.

6

7

8

9   **METHODS**

10   **Growth and harvest of *S. meliloti* for Ribo-seq**

11   *S. meliloti* 2011 (Casse et al. 1979) was first cultivated on TY (5 g of BactoTryptone, 3 g of

12   Bacto-yeast extract, and 0.3 g of CaC_2 per liter) agar plates (Beringer 1974). The plate cultures

13   were used to inoculate liquid cultures, which were grown semi-aerobically (routinely, 30 ml

14   of medium in a 50 ml Erlenmeyer flask under constant agitation at 140 rpm) at 30 °C in GMS

15   minimal medium (10 g of D-mannitol, 5 g of sodium glutamate, 5 g of K_2HPO_4, 0.2 g of $MgSO_4$

16    $\times 7H_2O$, and 0.04 g of $CaCl_2$ per liter; trace elements: 0.05 mg of $FeCl_3 \times 6H_2O$, 0.01 mg of H_3Bo_3,

17   0.01 mg of $ZnSO_4 \times 7H_2O$, 0.01 mg of $CoCl_2 \times 6H_2O$, 0.01 mg of $CuSO_4 \times 5H_2O$, 1.35 mg of $MnCl_2$,

18   and 0.01 mg of $Na_2MoO_4 \times 2H_2O$ per liter; 10 μg of biotin and 10 mg of thiamine per liter)

19   (Zevenhuizen and van Neerven 1983). As the strain exhibits chromosomally encoded

20   streptomycin resistance, 250 μg/ml streptomycin was added to the media. For Ribo-seq

21   sample preparation, cells corresponding to 40 OD_{600} equivalent units were harvested after

22   rapid chilling in an ice bath to halt cell growth and translation. In brief, cultures in the

23   exponential phase (OD_{600nm} 0.5) were rapidly placed in a pre-chilled flask in an ice-water bath

24   and incubated with gentle shaking for 3 min. Cells were then immediately pelleted by

25   centrifugation (10 min at 6000 ×g) before snap-freezing in liquid N_2. Before centrifugation, a

26   culture aliquot was withdrawn for total RNA analysis, mixed with 0.2 vol stop mix (5% buffer-

27   saturated phenol [Roth] in 95% ethanol), and snap-frozen in liquid N_2. Even though

28   translation elongation inhibitors have been extensively used in both eukaryotic and bacterial

29   Ribo-seq workflows, using such chemicals can introduce bias into Ribo-seq coverage

30   (Gerashchenko and Gladyshev 2014; Mohammad et al. 2019). Therefore, we chose to perform

31   Ribo-seq without these inhibitors because we were able to recover sufficient polysomes using

32   the fast-chilling method (see **Fig. 1**).

Preparation of ribosome footprints

Ribo-seq was performed as previously described (Oh et al. 2011), with some modifications. In brief, cell pellets were resuspended with cold lysis buffer (1 M NH_4Cl, 150 mM $MgCl_2$, 20 mM Tris-HCl, 5 mM $CaCl_2$, 0.4% Triton X-100, 150 U DNase I [Fermentas], and 1000 U RNase Inhibitor [MoloX, Berlin] at pH 8.0) and lysed by sonication (constant power 50%, duty cycle 50%, and 3 × 30 s cycles with 30 s cooling on a water-ice bath between each sonication cycle to avoid heating of the sample). The lysate was clarified by centrifugation at 10,000 × g for 12 min at 4 °C. Approximately 15 A_{260} of lysate 200 U of RNase I (Thermo Fisher Scientific) was added. Polysome digestion was performed at 25 °C with shaking at 650 rpm for 90 min. A mock-digested control (no enzyme added) was performed in parallel to confirm the presence of polysomes in the lysate. To analyze polysome profiles and recover digested monosomes, we layered 15 A_{260} units onto a linear 10%–55% sucrose gradient prepared in 4X gradient buffer (10X gradient buffer: 100 mM $MgCl_2$, 200 mM Tris-HCl, 1 M NH_4Cl, and 20 mM dithiothreitol [DTT] at pH 8.0) in an ultracentrifuge tube (13.2 mL Beckman Coulter SW-41). Gradients were centrifuged in a SW40-Ti rotor at 35,000 rpm for 2 h and 30 min at 4 °C in a Beckman Coulter Optima XPN-80 ultracentrifuge. Gradients were processed using a gradient station (IP, Biocomp Instruments) fractionation system with continuous absorbance monitoring at 254 nm to resolve ribosomal subunit peaks. The 70S monosome fractions were collected and subjected to RNA extraction to purify the RNA footprints. RNA was extracted from fractions or cell pellets for total RNA using hot phenol-chloroform-isoamyl alcohol (25:24:1, Roth) or hot phenol (Roth), respectively, as previously described (Sharma et al. 2007; Venturini et al. 2020). Ribosomal RNA (rRNA) was depleted from 5 μg of DNase I-digested total RNA by subtractive hybridization with the Pan-Bacteria riboPOOLs (siTOOLs, Germany) according to the manufacturer's protocol with Dynabeads MyOne Streptavidin T1 beads (Invitrogen). Total RNA was fragmented with an RNA fragmentation reagent (Ambion). Monosome RNA and fragmented total RNA were size selected (26–34 nt) on 15% polyacrylamide/7 M urea gels, as previously described (Ingolia et al. 2012) using RNA oligonucleotides NI-19 and NI-20 as guides. RNA was cleaned and concentrated by isopropanol precipitation with 15 μg of GlycoBlue (Ambion) and dissolved in H_2O. cDNA libraries were prepared by Vertis Biotechnologie AG (Freising, Germany) using the adapter ligation protocol without fragmentation. First, an oligonucleotide adapter was ligated to the 3′ end of the RNA molecules. First-strand cDNA

synthesis was performed using M-MLV reverse transcriptase and the 3′ adapter as the primer. The first strand of cDNA was purified, and the 5′ Illumina TruSeq sequencing adapter was ligated to the 3′ end of the antisense cDNA. The resulting cDNA was PCR-amplified to approximately 10–20 ng/µl using a high-fidelity DNA polymerase. The DNA was purified using the Agencourt AMPure XP kit (Beckman Coulter Genomics) and analyzed by capillary electrophoresis. The primers used for PCR amplification were designed for TruSeq sequencing according to the instructions of Illumina. The following adapter sequences flank the cDNA inserts: TruSeq_Sense_primer: (NNNNNNNN = i5 Barcode for multiplexing) 5′-AATGATACGGCGACCACCGAGATCTACAC-NNNNNNNN-ACACTCTTTCCCTACA CGACGCTCTTCCGATCT-3′; TruSeq_Antisense_primer: (NNNNNNNN = i7 Barcode for multiplexing) 5′-CAAGCAGAAGACGGCATACGAGAT-NNNNNNNN-GTGACTGGAGTTCAGACGTGT GCTCTTCCGATCT-3′. cDNA libraries were pooled on an Illumina NextSeq 500 high-output flow cell and sequenced in single-end mode (75 cycles, with 20 million reads per library) at the Core Unit SysMed at the University of Würzburg.

Ribo-seq data analysis

S. meliloti Ribo-seq data were processed and analyzed using the published HRIBO workflow (version 1.6.0) (Gelhausen et al. 2021), which has previously been used for the analysis of bacterial Ribo-seq data (Venturini et al. 2020). In brief, sequencing read files were processed with a snakemake (Köster and Rahmann 2012) workflow, which downloads all required tools from bioconda (Grüning et al. 2018) and automatically determines the necessary processing steps. Adapters were trimmed from the reads with cutadapt (version 2.1) (Martin 2011) and then mapped against the *S. meliloti* 2011 genome with segemehl (version 0.3.4) (Otto et al. 2014). Reads corresponding to rRNA and other multiply mapping reads were removed with SAMtools (version 1.9) (Li et al. 2009). Quality control was performed by creating read count statistics for each processing step and RNA class with Subread featureCounts (1.6.3) (Liao et al. 2014). All processing steps were analyzed with FastQC (version 0.11.8) (Wingett and Andrews 2018), and the results were aggregated with MultiQC (version 1.7) (Ewels et al. 2016). Summary statistics are shown in **Table S1**.

Read coverage files were generated with HRIBO using different full-read mapping approaches (global or centered) and single-nucleotide mapping strategies (5′ or 3′ end).

1   Read coverage files using two different normalization methods were created (mil and

2   min). For the mil normalization, read counts were normalized by the total number of

3   mapped reads within the sample and scaled by a per-million factor. For the min

4   normalization, the read counts were normalized by the total number of mapped reads

5   within the sample and scaled by the minimum number of mapped reads among all

6   analyzed samples. The coverage files generated using the min normalization and the

7   global mapping (full read) approach were used for genome browser visualization.

8   Metagene analysis of ribosome density at start codons was performed as previously

9   described (Becker et al. 2013).

10   **Ribo-seq-based ORF prediction, filtering, and manual curation**

11   ORFs were called with an adapted variant of REPARATION (Ndah et al. 2017) using blast

12   instead of usearch (see https://github.com/RickGelhausen/REPARATION_blast) and

13   DeepRibo (Clauwaert et al. 2019). In addition, generic feature format (GFF) track files with

14   the same information were created for in-depth manual genome browser inspection, as

15   well as GFF files showing potential start and stop codons and ribosome binding site

16   information. Summary statistics for all available GenBank annotated and merged novel

17   ORFs detected by REPARATION and DeepRibo were computed in a tabularized form,

18   including, among other values, translation efficiency (TE), RPKM (reads per kilobase of

19   transcript per million mapped reads) normalized read counts, codon counts, and

20   nucleotide and aa sequences (see **Table S2**). Annotated sORFs were classified as translated

21   if they fulfilled an arbitrary mean TE cut-off of $\geq$ 0.5 and RNA-seq and Ribo-seq RPKM of $\geq$

22   10 (cut-offs chosen based on the lowest TE and RPKM values associated with housekeeping

23   genes [i.e., ribosomal protein genes] and the genes detected by proteomics). To identify

24   strong candidates for novel sORFs, we inspected HRIBO ORF predictions from DeepRibo

25   and REPARATION. As DeepRibo is prone to a high rate of false positives (Gelhausen et al.

26   2022), we first generated a reasonable set of potential novel sORFs by applying the

27   following expression cut-off filters: mean TE of $\geq$ 0.5 and RNA-seq and Ribo-seq RPKM of

28     $\geq$10 (in both replicates) based on the 85 positively labeled translated sORFs (see **Fig. 3**).

29   In addition, novel translated sORF candidates were required to be predicted by DeepRibo

30   with a prediction score of > −0.5 that allows for ORF candidate ranking (Clauwaert et al.

31   2019). The filtered sORFs were then subjected to manual curation, that is, inspection of the

32   Ribo-seq coverage in a genome browser. To assert translation, we considered the evenness

1   of the Ribo-seq coverage, its restriction to the predicted ORF, and the high read coverage

2   in the footprint library compared with the corresponding transcriptome library. We

3   created an interactive web-based genome browser using JBrowse (http://www.bioinf.uni-

4   freiburg.de/ribobase) (Buels et al. 2016), where the coverage files for the Ribo-seq

5   replicates, the annotation, and the predicted sORF can be visualized.

Sample preparation for MS

7   For MS analysis, cells of 1.5 l of an *S. meliloti* culture (OD$_{600nm}$ 0.5) were harvested by centrifugation

8   at 6,000 rpm and 4°C. The cell pellet was resuspended in 30 ml of buffer containing 20 mM Tris,

9   150 mM KCl, 1 mM MgCl$_2$, and 1 mM DTT at pH 7.5. After lysis by sonication and centrifugation

10   at 13,000 rpm for 30 min at 4°C, the cleared lysates were frozen in liquid nitrogen and stored at

11   −80 °C. To generate a highly comprehensive small protein dataset, we used three

12   complementary approaches for sample preparation: 1) tryptic in-solution digest of all

13   proteins in the sample, 2) solid-phase enrichment (SPE) of small proteins without any

14   subsequent digestion, and 3) SPE of small proteins with subsequent digestion using Lys-C.

15   Sample preparation was performed as previously described (Bartel et al. 2020) with some

16   modifications. In brief, samples for tryptic in-solution digests were reduced and alkylated

17   before trypsin was added in an enzyme-to-protein ratio of 1:100, and samples were

18   incubated at 37 °C for 14 h. The digest was stopped by acidifying the mixture with HCl. For

19   SPE, samples were loaded on an equilibrated column packed with an 8.5 nm pore size,

20   modified styrene-divinylbenzene resin (8B-S100-AAK, Phenomenex), which was then

21   washed to remove large proteins. The enriched small protein fraction was eluted with 70%

22   (v/v) acetonitrile and evaporated to dryness in a vacuum centrifuge. The SPE samples were

23   either directly used for MS or in-solution digested as described above but with Lys-C instead

24   of trypsin.

Generation of standard and custom iPtgxDBs to identify novel SEPs

26   iPtgxDBs were generated based on the *S. meliloti* 2011 ASM34606v1 reference genome

27   sequence as described (Omasits et al. 2017). Annotations from several reference genome

28   centers and/or releases (GenBank 2014, RefSeq2017, Genoscope), two *ab initio* gene

29   predictions (Prodigal, ChemGenome), and *in silico* ORF predictions were hierarchically

30   integrated for a trypsin-specific iPtgxDB as previously detailed (Melior et al. 2020),

31   (https://iptgxdb.expasy.org/database/annotations/s-meliloti-tryptic; see **Table S3.1**). To

32   capture data from all three experimental approaches, two more iPtgxDBs were created in a

similar fashion using command-line utilities. While default settings were used to create the trypsin-specific iPtgxDB, for the LysC-specific iPtgxDB, the regular expression "(K)(.)" was used, allowing cleavage after every lysine. The iPtgxDB for the experiments without protease digestion was generated with a regular expression that did not allow any cleavages. In addition, three 20-fold smaller custom iPtgxDBs were created to improve search statistics/predictive potential. For these, instead of adding the Chemgenome and *in silico* predictions, 266 selected Ribo-seq translation products identified from the sORF prediction tools DeepRibo (Clauwaert et al. 2019) and Reparation (Ndah et al. 2017), as well as manual analysis, were converted to GFF format using a custom Python script and integrated along with the RefSeq, GenBank, Genoscope, and Prodigal predictions to create the respective iPtgxDBs (**Tables S3.3** and **S3.4**). All six iPtgxDBs (downloadable from https://iptgxdb.expasy.org) also contained sequences of common laboratory contaminants (116 from CrapOme and 256 from the Functional Genomics Center Zurich). All peptides implying potentially novel proteins were subjected to a PeptideClassifier analysis (Qeli and Ahrens 2010) extended for proteogenomics in prokaryotes (Omasits et al. 2017). This procedure ensures that i) only unambiguous peptides were considered (class 1a) or ii) annotation cluster-specific cases can be distinguished: Class 2a peptides imply a subset of all possible proteoforms (e.g., like an extension, reduction), class 2b peptides imply all isoforms, which means that the gene encoding the proteoforms, but not a specific proteoform, was identified.

MS analysis

Samples were loaded on an EASY-nLC 1200 (Thermo-Fisher Scientific) equipped with an in-house-built 20 cm reversed-phase column packed with 3 μm Reprosil-Pur 120 C18-AQ (Dr. Maisch) and an integrated emitter tip. Peptides were eluted by a 156 min non-linear gradient of solvent B (0.1% v/v acetic acid in acetonitrile) and injected online in an Orbitrap Velos (Thermo-Fisher Scientific). The survey scans were acquired in the Orbitrap (300–1700 Th; 60,000 resolution at 400 m/z; $1 \times 1e_6$ predictive automatic gain control target; activated lock mass correction). After collision-induced dissociation with a normalized collision energy of 35, fragment spectra were recorded in the LTQ (mass range dependent on precursor m/z; $3 \times 1e_4$ predictive automatic gain control) for the 20 most abundant ions. Fragmented ions were dynamically excluded from fragmentation for 30 s.

11

1   DB searches were performed with Sorcerer-SEQUEST 4 (Sage-N Research, Milpitas, USA), allowing two missed cleavages for samples derived from tryptic in solution digest or LysC digested SPE samples and with non-specified enzymes for SPE samples without proteolytic digest. No fixed modifications were considered, and oxidation of methionine was considered a variable modification. The mass tolerance for precursor ions was set to 10 ppm, and the mass tolerance for fragment ions was set to 1.0 Da. Validation of MS/MS-based peptide and protein identification was performed with Scaffold V4.8.7 (Proteome Software, Portland, USA), and peptide identifications were accepted if they exhibited at least deltaCn scores of > 0.1 and XCorr scores of > 2.2, 3.3, and 3.75 for doubly, triply, and all high-charged peptides, respectively. Identifications for proteins of > 15 kDa were only accepted if at least two unique peptides were identified. Proteins that contained ambiguous, non-unique peptides and could not be differentiated based on MS/MS analysis alone were grouped to satisfy the principles of parsimony (Sorcerer-SEQUEST). Identifications for annotated proteins of < 15 kDa were accepted if at least one unique peptide was identified with at least two peptide spectrum matches (PSMs). To identify novel proteins, we required additional PSM evidence from predictions as described before (Varadarajan et al. 2020a, 2020b), that is, 3 PSMs for *ab initio* predictions and 4 PSMs from *in silico* predictions. Here, we also allowed *in silico* candidates with 3 PSMs if they were observed in each of the three replicates. Similar to the RefSeq annotated proteins, novel proteins longer than 150 aa required two unique peptides (however, these were not the focus of this study). The application of these filter criteria kept the protein false discovery rate (FDR) below 1%. To facilitate overview and comparison, we integrated MS-identified proteins, Ribo-Seq, and Western blot analysis data in a "master table" (**Table S4**).

Cloning procedures

The oligonucleotides (Microsynth) used for cloning are listed in **Table S5**. Routinely, FastDigest Restriction Endonucleases and Phusion polymerase (Thermo Fisher Scientific) were used. PCR products were first ligated into pJet1.2/blunt (CloneJet PCR Cloning Kit, Thermo Fisher Scientific) and transformed into *E. coli* DH5-alpha. Subsequently, inserts were subcloned in conjugative plasmids originating from pSRKGm (Khan et al. 2008). Insert sequences were analyzed by Sanger sequencing with plasmid-specific primers (Microsynth Seqlab). *E. coli* S17-1 was used to transfer the plasmids to *S. meliloti* 2011 by diparental conjugation (Simon et al. 1983).

1　Plasmid pSW2 was used to clone the candidate sORFs. It was constructed using pRS1, a

2　derivative of pSRKGm, in which the *E. coli lac* module was exchanged for a multiple

3　cleavage site-containing cloning site for the restriction endonucleases NheI, HindIII, XbaI,

4　SpeI, BamHI, PstI, and EcoRI. First, a transcription terminator T_{rrn} from *Bradyrhizobium*

5　*japonicum* USDA 110 was cloned into the EcoRI restriction site of pRS1. For this, the

6　terminator containing sequence was amplified with the forward primer Bj-Trrn-Fw-2019

7　and the reverse primer Bj-Trrn-Rv-2019 using plasmid pJH-O1 as a template (Čuklina et

8　al. 2016). In the PCR product, an EcoRI restriction site was present downstream of the

9　forward primer sequence. This restriction site and that in the reverse primer were used

10　for the transcription terminator cloning. A clone with the desired orientation was

11　selected, and the plasmid was named pRS1-Trrn (**Fig. S1**). Double-stranded DNA

12　encoding a sequential peptide affinity (SPA) tag, which is composed of the calmodulin-

13　binding peptide and three modified FLAG sequences separated by a TEV protease

14　cleavage site (Zeghouf et al. 2004), was then cloned between the BamHI and EcoRI

15　cleavage sites of pRS1-Trrn. The SPA-tag encoding sequence was designed without an

16　ATG codon, without rare codons, and with Gly-Gly-Gly-Ser linker codons at the 5′ end and

17　adapted to the high GC content of *S. meliloti*. It was generated synthetically by Eurofins

18　and provided on plasmid pEX-A128, which was used as a template for PCR amplification

19　with primers SmSPA-Ct-BamFW and SmSPA-Ct-EcoRv. The resulting plasmid pSW1 can

20　be used to clone an sORF in frame with the SPA-encoding sequence and under the control

21　of its own promoter. Here, pSW1 was used to clone the promoter P_{sinI} between the NheI

22　and XbaI restriction sites. The promoter sequence (McIntosh et al. 2008) was amplified

23　using primers NheI-PsinI-FW and XbaI- PsinI-RV and *S. meliloti* 2011 genomic DNA as a

24　template. The resulting pSW2 plasmid was used to clone candidate sORFs, each with a 15-

25　nt upstream region potentially harboring a Shine-Dalgarno sequence between the XbaI

26　and BamHI restriction sites (**Fig. S1**). In total, 20 sORF::SPA fusions were cloned and

27　tested by Western blot analysis. The corresponding plasmids were designated from

28　pSW2-SEP1 to pSW2-SEP20.

29　**Western blot analysis**

30　Exponentially grown *S. meliloti* cells (OD_{600nm} 0.5; minimal medium) were harvested (3,500

31　×g for 10 min at 4 °C) and resuspended in an SDS-loading buffer. After incubation for 5

32　min at 95 °C, the crude lysate proteins were separated by Tricine-SDS PAGE (16%) and

33　blotted onto a PVDF membrane (Amerham™Hybond™, 0.2 µM PVDF; GE Healthcare Life

13

1   Science, Chalfont St Giles, Great Britain) as described (Schägger 2006). For detection,

2   monoclonal ANTI-FLAG M2-Peroxidase (HRP) antibodies (Merck, Darmstadt, Germany)

3   and Lumi-Light Western-Blot-Substrate (Roche, Basel, Schweiz) were used. Signal

4   visualization was performed with a chemiluminescence imager (Fusion SL4, Vilber,

5   Eberhardzell, Germany). For fractionation, the cell pellets were resuspended in TKMDP

6   buffer containing 20 mM Tris-HCl, 150 mM KCl, 1 mM $MgCl_2$, 1 mM DTT, and one protease

7   inhibitor cocktail tablet at pH 7.5 (Sigma Aldrich, St. Louis, USA). Lysates prepared by

8   three passages in a French press at 1,000 psi were cleared by centrifugation at 14,000 ×g

9   for 30 min at 4 °C. The supernatant was subjected to ultracentrifugation at 100,000 ×g for

10   1 h at 4 °C. The supernatant (S100 fraction) was then removed, and the P100 pellet was

11   resuspended in the same volume of TKMDP buffer.

12   **Conservation and domain search analyses**

13   The identification of novel small protein homologues was performed using Blastp and

14   tBlastn searches in bacteria on the National Center for Biotechnology Information DB

15   (https://blast.ncbi.nlm.nih.gov/Blast.cgi). The protein sequences for novel protein

16   candidates identified by Ribo-seq and/or MS were used as query sequences. For tBlastn,

17   the following parameters were used: the filter for low complexity regions off, a seed length

18   that initiates an alignment (word size) of 6, 60% coverage of the query sequence with at

19   least 40% identity, an E-value (Expect value) of ≤100 to capture all potential orthologs, and

20   an E-value between 0.01 and 1 for high-confidence hits (Allen et al. 2014). Moreover, novel

21   small proteins discovered in this study were further analyzed for secondary structure and

22   predicted protein domains and predictions of lipoproteins, as well as potential subcellular

23   localization using predictions from the Phyre2 v2.0

24   (http://www.sbg.bio.ic.ac.uk/~phyre2/), LipoP-1.0

25   (https://services.healthtech.dtu.dk/service.php?LipoP-1.0) TMHMM v2.0

26   (https://services.healthtech.dtu.dk/service.php?TMHMM-2.0), and PSORTb v3.0.2

27   servers (https://www.psort.org/psortb/).

28   **Data availability**

29   The MS-based proteomics data were deposited to the ProteomeXchange Consortium at the

30   PRIDE partner repository, with dataset identifier PXD034931. The iPtgxDBs can be

31   downloaded from https://iptgxdb.expasy.org/. Ribo-seq and RNA-seq data were deposited

32   in GEO, with accession number GSE206492. The Ribo-seq and RNA-seq data of *S. meliloti*

1   2011 can be viewed with an interactive online JBrowse instance (http://www.bioinf.uni-

2   freiburg.de/ribobase).

3

RESULTS

Establishing Ribo-seq in *S. meliloti* to map its translatome

To provide a genome-wide map of translated annotated sORFs and to reveal new sORFs in the plant symbiont *S. meliloti*, we first adapted the Ribo-seq protocol (Oh et al. 2011) to this organism (**Fig. 1A**). For this purpose, several steps, including cell harvest, lysis, and footprint generation, were optimized (see Methods). *S. meliloti* 2011 cells were grown to the mid-log phase in minimal medium, and samples were rapidly cooled and harvested to avoid polysome run-off. Polysome profile analysis after lysate fractionation on a sucrose gradient showed successfully captured translating ribosomes (**Fig. 1B**, black profile). The mRNA should be ribonucleolytically digested outside ribosomes to produce ribosome footprints. Since the broad-range ribonuclease RNase I, which is often used for eukaryotic Ribo-seq analysis, is inactive on polysomes from enteric bacteria (Bartholomäus et al. 2016), most prokaryotic Ribo-seq protocols mainly use micrococcal nuclease (MNase) instead. However, MNase preferentially cleaves at pyrimidines, introduces periodicity artifacts, and generates footprints that are more heterogeneous in length than those from RNase I (Ingolia 2016; Vazquez-Laslop et al. 2022). Therefore, we used RNase I to convert *S. meliloti* polysomes into monosomes (**Fig. 1B**) and to generate ribosome footprints (**Fig. 1C–1E**). By comparing Ribo-seq read coverage data and expression signals from a paired RNA-seq library generated from fragmented total RNA, features, such as coding potential, ORF boundaries, and 5′ and 3′ UTRs, can be defined (**Fig. 1C–1E**).

Inspection of Ribo-seq coverage for translated ORFs and known non-coding transcripts further demonstrated the successful setup of Ribo-seq in *S. meliloti.* For example, the protein-coding genes *rpsO* and *icd* showed higher cDNA read coverage in the Ribo-seq library compared with the paired RNA-seq library (**Fig. 1C**), whereas the RNase P RNA gene *rnpB* showed high cDNA read coverage only in the RNA-seq library (**Fig. 1D**). Furthermore, the cDNA read coverages of the 5′ and 3′ UTRs of *rpsO* and *icd* were higher in the RNA-seq library than in the Ribo-seq library (**Fig. 1C**), showing successful digestion of non-translated or

15

1 unprotected mRNA regions by RNase I. Similarly, the protein-coding polycistronic *fixN1OQP*

2 mRNA showed high read coverage in the Ribo-seq library along its four ORFs. In contrast, the

3 5′ leader and 3′ trailer mainly showed coverage in the RNA-seq library, suggesting that they

4 were digested by RNase I (**Fig. 1E**).
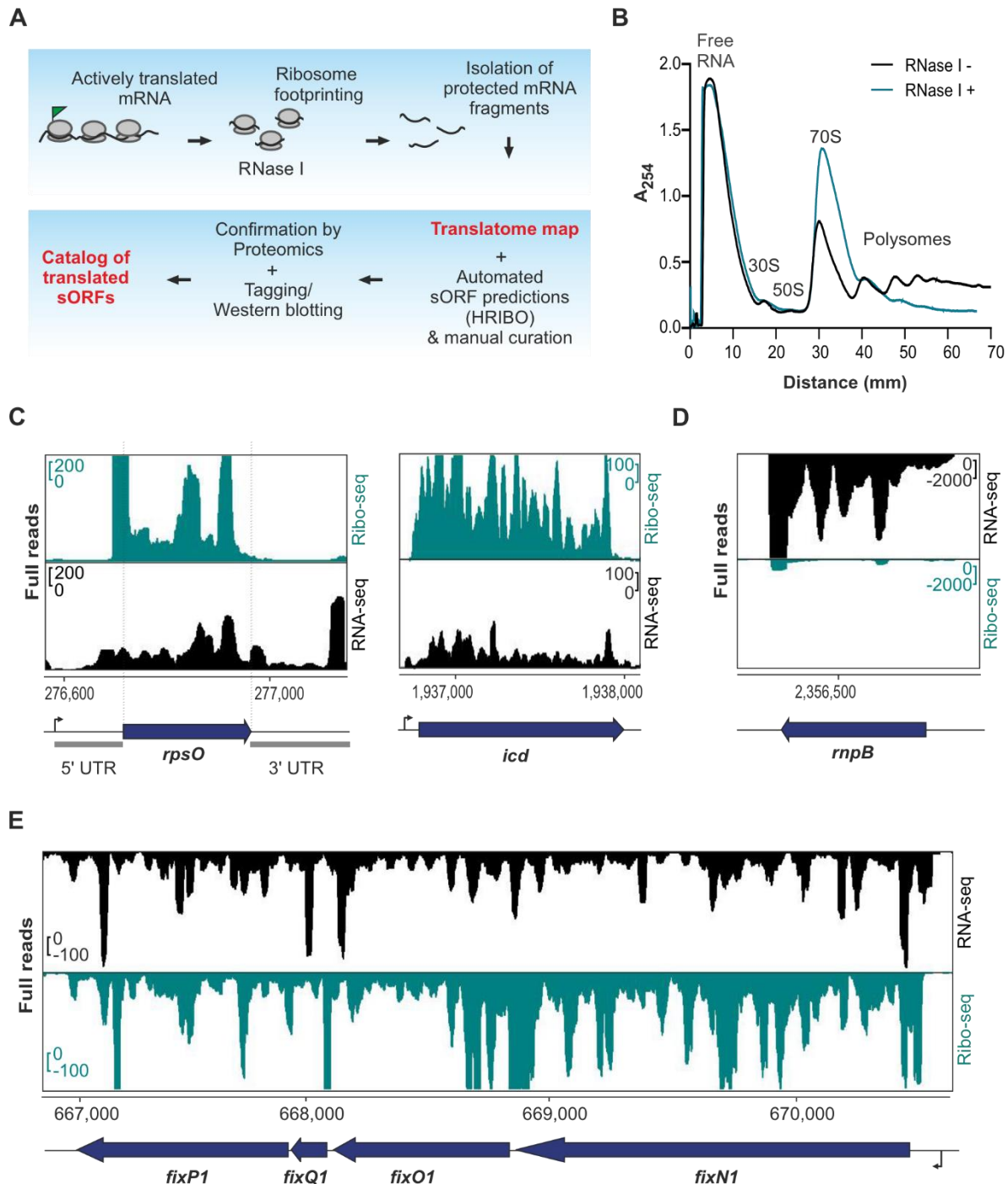
6 **Figure 1**. **Establishment of ribosome profiling (Ribo-seq) for *Sinorhizobium meliloti*. (A)**

7 Schematic Ribo-seq workflow to map the *S. meliloti* 2011 translatome. Translating ribosomes

8 (indicated by the polysome fraction) were first captured on the mRNAs. Unprotected mRNA regions

1   were digested by RNase I, converting polysomes to monosomes. Approximately 30-nt-long footprints

2   protected by and co-purified with 70S ribosomes were then subjected to cDNA library preparation

3   and deep sequencing to identify the translatome under the used conditions. The small proteome was

4   identified using HRIBO automated predictions and manual curation. Mass spectrometry and Western

5   blot analysis of recombinant, tagged small open reading frame (sORF)-encoded proteins were used to

6   validate the translated sORFs. **(B)** Sucrose gradient fractionation of the lysates. Cells were harvested

7   at the exponential growth phase by a fast-chilling method to avoid polysome run-off. RNase I digestion

8   led to enrichment of monosomes (70S peak in the green profile) in contrast to the untreated sample

9   (Mock, black profile). Absorbance at 254 nm was measured. **(C)** Integrated genome browser

10   screenshots depicting reads from Ribo-seq and RNA-seq libraries for two annotated ORFs: *rpsO*

11   encoding ribosomal protein S15 and *icd* encoding isocitrate dehydrogenase. They show read coverage

12   enrichment in the Ribo-seq library along their coding parts in contrast to the RNA-seq library but not

13   in the ribosome-non-protected regions (UTRs). The UTRs of *rpsO* are marked. **(D)** Read coverage for

14   *rnpB* corresponding to the housekeeping RNase P RNA. Reads are mostly restricted to the RNA-seq

15   library, suggesting that this RNA is not translated. **(E)** The *fixN1OQP* operon shows read coverage in

16   both the RNA-seq library and Ribo-seq library, the latter indicating that this operon contains

17   translated genes. Genomic locations and coding regions are indicated below the image. Bent arrow

18   indicates the transcription start site based on (Sallet et al. 2013)**.**

19

20   The high ribosome density in the Ribo-seq library, which covers the 14 and 12-nt-long

21   intergenic regions between *fixN1 - fixO1* and *fixO1 - fixQ1,* probably represents the footprints

22   of ribosomes that terminate the translation of the upstream ORF and initiate the translation

23   of the downstream ORF. Such events are slower than elongation at most codons in an ORF

24   (Oh et al. 2011). The latter example indicates the translation of the sORF *fixQ1*, which encodes

25   a 50 aa protein (**Fig. 1E**).

26   Metagene analysis of ribosome occupancy near all annotated start codons (i.e., ATG, GTG, and

27   TTG) showed an enriched ribosome density at the −16 nt upstream (mapping of the 5′ ends

28   of the footprints) and at +16 nt downstream (mapping of the 3′ ends of the footprints) (**Fig.**

29   **S2A and S2B;** note: +1 is the first nucleotide of the start codon), in line with the expected

30   position of initiating ribosomes waiting to engage in elongation. This feature is a

31   characteristic of translated bacterial ORFs identified by Ribo-seq (Mohammad et al. 2019; Oh

32   et al. 2011). In contrast to MNase-generated Ribo-seq libraries in *E. coli* (Mohammad et al.

33   2019), no differences in the assignment of ribosome position using the 5′ end or 3′ end

1   mapping approaches were observed (**Fig. S2A** and **S2B**). In the Ribo-seq libraries, we

2   consistently recovered footprints between 27–33 nt (mean at 30 nt), with enrichment of

3   ribosome density strongest at the start codon for the 32 nt footprints (**Fig. S2C** and **S2D**).

4

5   **Ribo-seq captures the translatome of *S. meliloti* and reveals features at the single gene**

6   **level**

7   By comparing the signals of the Ribo-seq and RNA-seq libraries, the TE (Ribo-seq/total RNA

8   coverage) can be estimated at a given locus. This method allowed us to derive a genome-wide

9   estimate of the translatome in minimal medium, where 3,758 of the 6,263 annotated coding

10   sequences (CDS) (60%; GenBank Annotation 2014) had a Ribo-seq signal above the

11   arbitrarily chosen TE cut-off of ≥ 0.5 and RNA-seq and Ribo-seq RPKM of ≥ 10 (see **Methods,**

12   **Fig. 2A, Table S6**). In contrast, the ORF prediction tools implemented in HRIBO (Gelhausen

13   et al. 2021, 2022) detected translation for 2,136 of the 3,758 ORFs (57%), suggesting an

14   average performance in predicting long translated ORFs in *S. meliloti* (**Fig. 2A, Table S6**).

15   Inspection of the TE for different annotated gene classes and untranslated mRNA regions (all

16   CDS, 5′ and 3′ UTRs, non-coding RNAs, and sORFs) revealed that annotated ORFs exhibited a

17   higher mean TE (TE ≥ 1) compared with non-coding genes, such as housekeeping RNA genes

18   (hkRNA, e.g., tmRNA, 6S, ffs, *rnpB* and *inc*A1/2 RNA, mean TE <1) (**Fig. 2B**), again

19   corroborating the ability of our Ribo-seq data to differentiate between coding and non-coding

20   genes. The 5′ UTR regions of translated mRNAs generally had a mean TE of ≥ 1, which possibly

21   resulted from protection from RNase I trimming of the −16 nt region upstream of the start

22   codon by the initiating ribosomes (**Fig. S2**). This feature was particularly prominent in the

23   leader regions of mRNAs with short 5′ UTRs, indicating that they are partially protected from

24   digestion by initiating ribosomes (**Fig. S3A**). In addition, some 5′ UTRs might contain

25   translated upstream sORFs, such as *trpL* upstream of *trpE* (marked in red in **Fig. 2D)** (Melior

26   et al. 2020). Although less pronounced than at the start codon, the translation-terminating

27   ribosome also protects a certain 3′ UTR region from RNase digestion (Oh et al. 2011),

28   explaining the slightly higher mean TE of 3′ UTRs (**Fig. 2B**). Furthermore, a few of the 3′ UTRs

29   might also contain translated downstream sORFs (**Fig. S3B;** Dodbele and Wilusz 2020; Wu et

30   al. 2020), which may explain the slightly higher mean TE of 3′ UTRs.

31
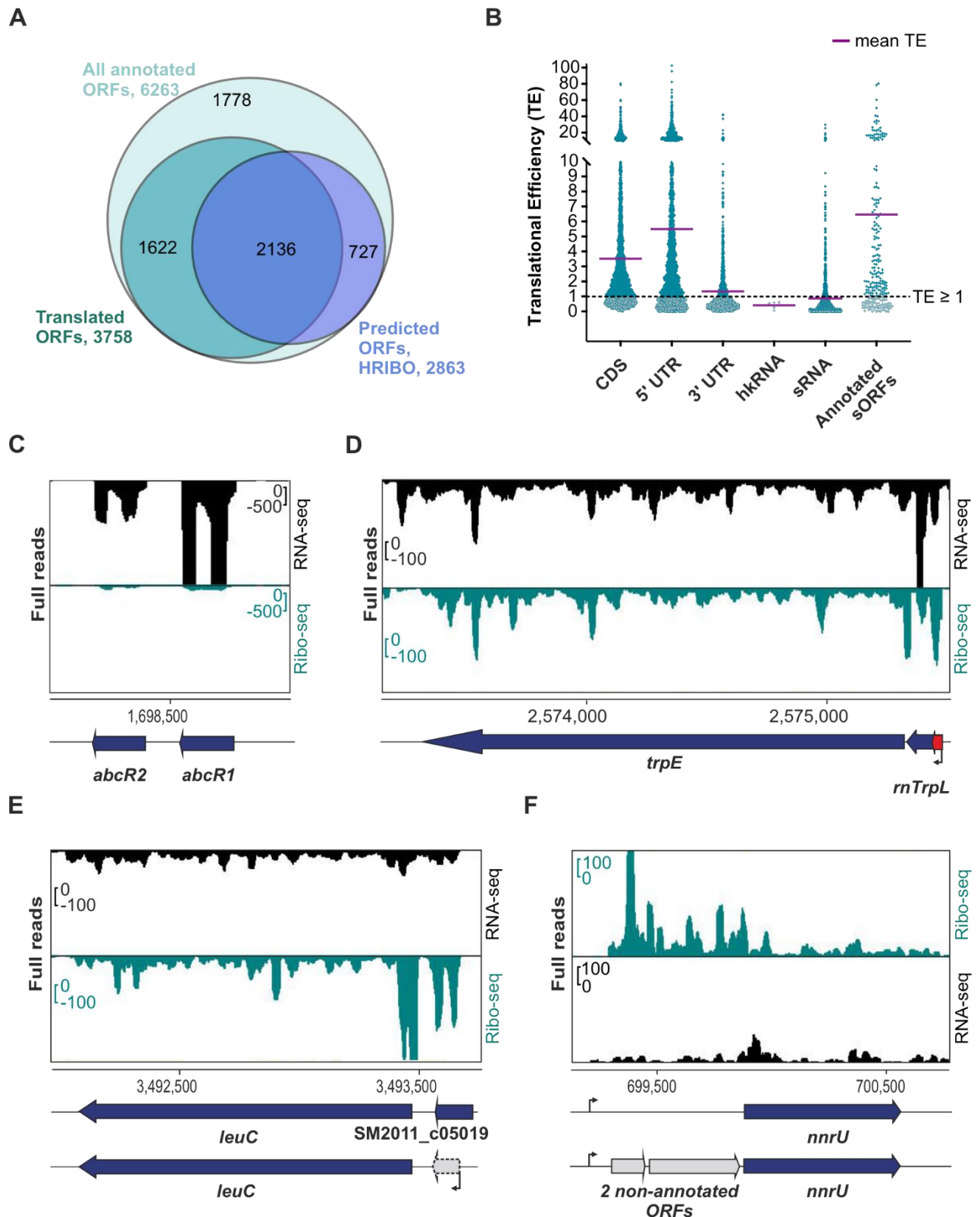
Figure 2. Ribosome profiling (Ribo-seq) captures the translatome of *Sinorhizobium meliloti* 2011 and reveals some features at the single-gene level. (A) Comparison of all annotated open reading frames (ORFs), annotated translated ORFs detected by Ribo-seq, and ORFs predicted to be translated by tools included in the HRIBO pipeline. To detect translation, we used the following parameters on the Ribo-seq data: TE of ≥ 0.5 and RNA-seq and Ribo-seq RPKM of ≥ 10. The numbers

19

1   of ORFs per category are shown and represented by area size. Diagrams were prepared with BioVenn

2   (www.biovenn.nl). **(B)** Scatter plot showing global TEs (TE = Ribo-seq/RNA-seq) computed from *S.*

3   *meliloti* Ribo-seq replicates for all annotated coding sequences (CDS), annotated 5′ and 3′ UTRs,

4   annotated housekeeping RNAs (hkRNA), annotated small RNAs (sRNAs) with (putative) regulatory

5   functions, and annotated sORFs encoding proteins of ≤ 70 amino acids (aa). The purple lines indicate

6   the mean TE for each transcript class. **(C)** Analysis of the two well-characterized sRNAs AbcR1 and

7   AbcR2 by Ribo-seq. These two sRNAs show read coverage, mostly in the RNA-seq library. **(D)** Ribo-

8   seq reveals the active translation of the *trpE* leader peptide peTrpL (14 aa, encoded by the leaderless

9   sORF *trpL* in the 5′ UTR (red arrow) and/or by the attenuator sRNA rnTrpL). In addition, the coverage

10 of the Ribo-seq library shows that the biosynthetic gene *trpE* is translated in minimal medium, as

11 expected. **(E)** Re-annotation of the annotated sORF SM2011_c05019 (50 aa). The actual annotation

12 does not fit the RNA-seq and Ribo-seq read coverages. HRIBO predicts a shorter leaderless sORF (38

13 aa) that corresponds to the read coverage in both libraries. **(F)** Two ORFs missing from the GenBank

14 (2014) annotation are revealed by Ribo-seq upstream of the *nnrU* gene related to denitrification.

15 Genomic locations and coding regions are indicated below the image. Bent arrows indicate

16 transcription start sites based on (Sallet et al. 2013).

17

18 Most of the annotated sRNAs had a mean TE of < 1, indicating that they are in fact non-coding,

19 such as the sRNAs AbcR1 (TE=0.2) and AbcR2 (TE=0.09) (**Fig. 2C**) (Torres-Quesada et al.

20 2013). However, some annotated sRNAs had a mean TE of ≥ 1, suggesting that they may be

21 small mRNAs or dual-function sRNAs (**Fig. S3C**). For example, **Fig. 2D** shows the recently

22 described dual-function sRNA rnTrpL (TE = 1.16), which corresponds to the tryptophan

23 attenuator and contains the *trpL* sORF encoding the functional 14 aa leader peptide peTrpL

24 (Melior et al. 2019; Melior et al. 2021). Since rnTrpL is a small, leaderless mRNA starting with

25 the AUG of *trpL*, **Fig. 2D** also exemplifies how our Ribo-seq analysis can capture leaderless

26 translated ORFs. Furthermore, as expected, we detected active translation of the biosynthetic

27 genes *trpE* and *leuC* under growth in minimal medium lacking tryptophan and leucine (**Fig.**

28 **2D** and **2E**).

29 Finally, we used our Ribo-seq data to curate the annotation of *S. meliloti*. For example, Ribo-

30 seq, RNA-seq data, and our computational ORF predictions based on Ribo-seq all indicated

31 that the start of the sORF SM2011_c05019 (50 aa) is likely located downstream of the current

32 annotation, implying a shorter sORF of 38 aa (**Fig. 2E**). Additional sORFs whose annotation

33 should be adjusted are reported in **Table S7**. Moreover, our data revealed additional ORFs

1   that should be added to the genome annotation. For example, the RNA-seq and Ribo-seq read

2   coverages indicate active expression (transcription and translation) upstream of the *nnrU*

3   gene. However, no gene was predicted in this region of the GenBank 2014 annotation.

4   HRIBO's prediction tools indicated the potential for two non-annotated ORFs encoding 51

5   and 132 aa proteins upstream of the *nnrU* gene (**Fig. 2F**). The 51 aa ORF is annotated in the

6   related *Sinorhizobium medicae* and *Ensifer adhaerens*, and in the latter, a homologous 142 aa

7   ORF is annotated between the 51 aa sORF and *nnrU*. Notably, while both ORFs were contained

8   in the *S. meliloti* RefSeq 2017 annotation, the 132 aa ORF was removed again from the latest

9   version (June 2022). This observation underlines the need for and value of integrative

10 approaches that can capture and consolidate reference genome annotations from different

11 annotation centers and even from different releases, which can differ substantially. The

12 iPtgxDB approach (Omasits et al. 2017) represents one strategy to readily capture and

13 visualize such differences, as we show here and for a number of additional cases below.

14

15 **Ribo-seq reveals translated annotated small proteins in *S. meliloti***

16 Among the 6,263 annotated CDS in the *S. meliloti* 2011 genome (the annotation from

17 GenBank 2014 has been used in the laboratory as a reference point for several years), 259

18 (roughly 4%) correspond to SEPs, with sizes ranging between 30 (the smallest annotated

19 SEP) and 70 aa (**Table S6**). To benchmark our Ribo-seq data for its capacity for global

20 identification of translated sORFs, we analyzed the Ribo-seq read coverage of these 259

21 annotated sORFs. By applying the TE of ≥ 0.5 and RNA-seq and Ribo-seq RPKM of ≥ 10

22 cut-off criteria, 131 of them were suggested to be translated (**Table S6**). However, we

23 further included an extensive manual inspection (see **Methods**) of the Ribo-seq read

24 coverage on top of these cut-offs to derive a very high-confidence dataset of 85 (33%)

25 translated sORFs (**Fig. 3A, Table S6**).

26 We then used this set of manually curated, translated sORFs as a benchmark sORF data

27 set to evaluate the performance of two machine learning-based, automated, Ribo-seq-

28 based ORF prediction tools included in our HRIBO pipeline (Gelhausen et al. 2021, 2022),

29 REPARATION (Ndah et al. 2017), and DeepRibo (Clauwaert et al. 2019). REPARATION

30 predicted the translation for 23 of the 85 benchmark sORFs (26%; **Fig. 3A**), even missing

31 some highly translated sORFs, such as those encoding ribosomal proteins

1   (SM2011_c04434 encoding 50S ribosomal protein L34, mean TE = 5.47) and proteins with

2   housekeeping functions (SM2011_c04884 encoding the anti-sigma factor, mean TE = 2.02,

3   and SM2011_c03850 encoding the heme exporter D, a cytochrome C-type biogenesis

4   protein, mean TE = 0.88). In contrast, DeepRibo predicted translation for 66 of the 85

5   benchmark sORFs (78%; **Fig. 3A**), indicating that it performed better in terms of detecting

6   translated sORFs from *S. meliloti* Ribo-seq data.

7
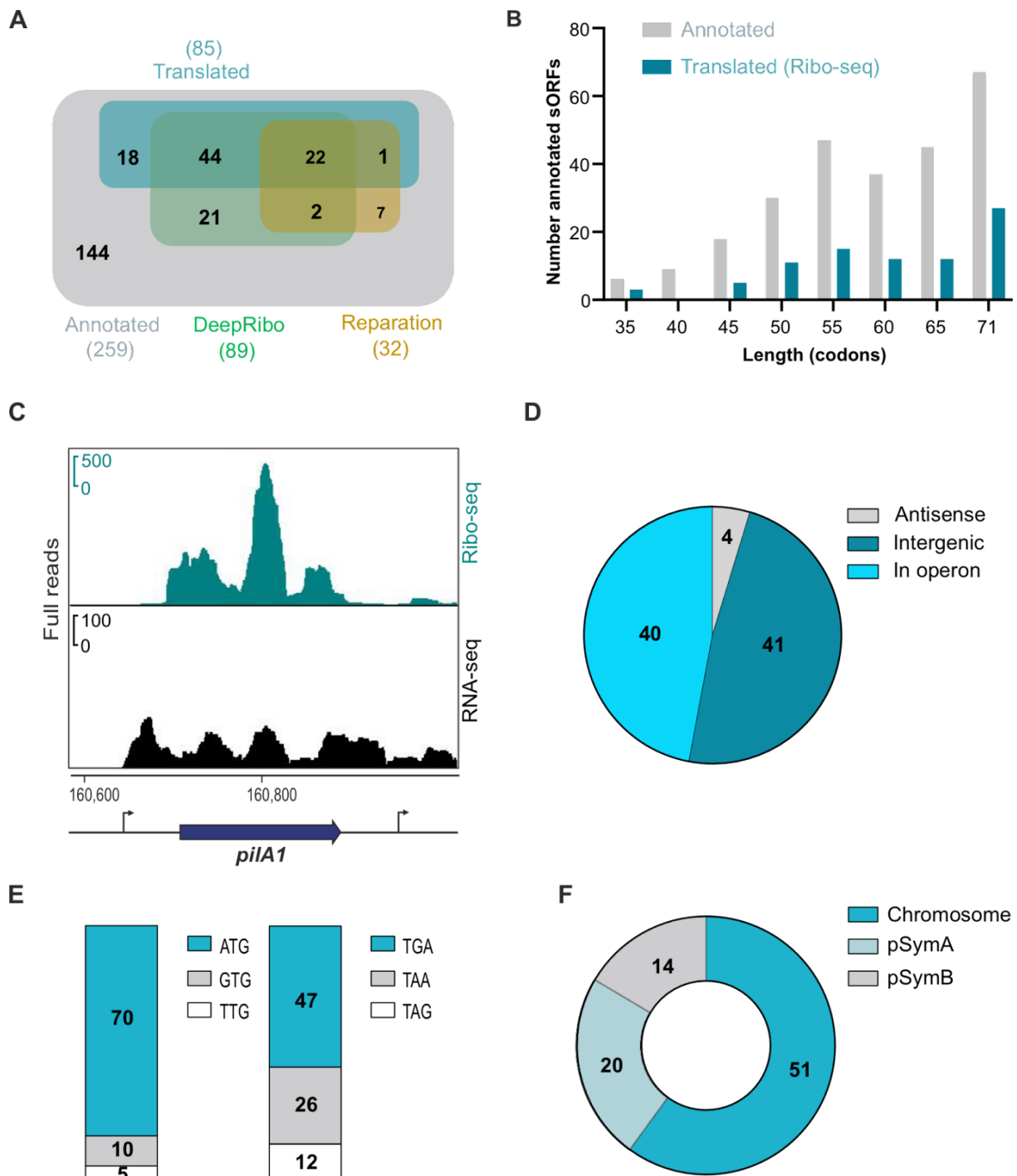
8

1 **Figure 3. Ribo-seq reveals translated annotated small open reading frames (sORFs) in**
2 ***Sinorhizobium meliloti* 2011. (A)** Venn diagrams showing the overlap between all annotated
3 sORFs (259 sORFs, GenBank 2014), the sORFs detected as translated by Ribo-seq (benchmark set,
4 TE of ≥ 0.5, RNA-seq and Ribo-seq RPKM of ≥ 10, and extensive manual curation), and sORFs
5 predicted by the automated ORF prediction tools Reparation or DeepRibo. **(B)** Histogram showing
6 the length distribution of the 85 annotated sORFs identified as translated by Ribo-seq in
7 comparison with the 259 annotated sORFs. **(C)** Integrated genome browser screenshot depicting
8 reads from the Ribo-seq and RNA-seq libraries for the annotated sORF *pilA1* (60 amino acids,
9 encoding a pilin subunit). The genomic position and the coding region are indicated below the
10 image. Bent arrows indicate transcription start sites based on (Sallet et al. 2013). **(D)** Genomic
11 context for the translated annotated sORFs relative to the annotated neighboring genes. **(E)** Start
12 (left) and stop (right) codon usage of the translated annotated sORFs. **(F)** Replicon distribution of
13 the translated annotated sORFs.

14

15 The majority of the 259 annotated (76%) and the subset of 85 translated sORFs (78%)
16 encode SEPs of ≥ 50 aa (**Fig. 3B**), in line with the expected poor annotation of very short
17 ORFs.

18 **Fig. 3C** shows read coverage from the Ribo-seq and RNA-seq libraries for the sORF
19 encoding a 60 aa pilin subunit (TE=23.3), which illustrates the successful digestion of
20 parts of the 5′ and 3′ UTR regions not covered by ribosomes, thus allowing us to define
21 sORF borders. In terms of type of genomic location, most of the translated annotated
22 sORFs are located in intergenic regions and operons, and only a few were found in
23 antisense transcripts (**Fig. 3D**). The vast majority of the translated annotated sORFs were
24 found to start with ATG, followed by GTG and TTG. The stop codon preference, although
25 less pronounced, was TGA > TAA > TAG (**Fig. 3E**). Finally, 60% of the 85 translated
26 annotated sORFs were located on the chromosome, 23.5% on the megaplasmid pSymA,
27 and 16.5% on the megaplasmid pSymB (**Fig. 3F**).

28

29 **Ribo-seq further expands the small proteome of *S. meliloti***

30 We then aimed to exploit the sensitivity of Ribo-seq to identify potential novel *S. meliloti*
31 2011 sORFs missing from GenBank annotation (2014) and thereby provide a nearly
32 complete catalog of its small proteome. The two machine learning-based, automated, Ribo-

23

seq-based ORF prediction tools integrated into the HRIBO pipeline produced a large number of predictions (approximately 15,000) for potential non-annotated sORFs (**Fig. 4A**), as previously shown in other bacterial species (Gelhausen et al. 2022). Given that these ORF prediction tools neither consider RNA-seq data nor TE but only utilize ribosome occupancy, we decided to filter the predictions for those with RNA-seq and Ribo-seq RPKM values of ≥10 and mean TE of ≥ 0.5. In addition, we applied a stringent cut-off for the DeepRibo score (see **Methods**) that allowed the ORF candidate ranking, which led to 266 candidates of translated non-annotated sORFs. Manual curation of all candidates based on their Ribo-seq coverage left us with a list of 54 non-annotated sORFs, which we proposed with high confidence to be translated during growth of *S. meliloti* in minimal medium (**Fig. 4A; Table S7**). Overall, the 54 non-annotated sORFs were shorter than the annotated ones: 33 of them (61%) correspond to SEPs with lengths between 10 and 49 aa, and nine of them (17%) represent SEPs shorter than 30 aa (the shortest annotated ORF in the *S. meliloti* annotation). A comparison of the length distribution of the 85 annotated and 54 non-annotated translated sORFs (**Fig. 4B**) illustrates the potential of Ribo-seq to detect very short translated sORFs.

The 54 non-annotated sORFs are encoded in diverse genomic contexts (**Fig. 4C**): 33% were located on annotated sRNAs, suggesting that these sRNAs are small mRNAs or dual-function sRNAs, 26% were in the intergenic regions, thus defining small mRNAs, and 20% were in the 5′ UTRs and may correspond to regulatory upstream ORFs (Evguenieva-Hackenberg 2022). Only a few were located in 3′ UTRs, on antisense transcripts and in an operon (**Fig. 4C**). Moreover, the majority of the 54 sORFs (63%) were located in the chromosome, 22% on pSymA, and 15% on pSymB (**Fig. 4D**), a distribution comparable to that of the annotated sORFs (**Fig. 3F**). Similar to the annotated sORFs, ATG was also the preferred start codon among the 54 non-annotated translated sORFs, and only five and four sORFs started with GTG or TTG, respectively; their stop codon preference was also similar to that of the annotated sORFs (**Table S6**). Importantly, as the iPtgxDB integrates and consolidates different reference genome annotations and various predictions, we could readily deduce that 11 of the 54 translated sORFs were contained in the 2017 RefSeq annotation, precisely matching their predicted start and stop codons (**Table S7**). Five candidates matched a RefSeq annotation, but they were shorter. One candidate matched the stop but was only 1 aa longer than the RefSeq annotation. Finally, three candidates matched a GenBank stop codon, but they were shorter than annotated (one of

24

1 which was in fact again removed in the RefSeq annotation). In summary, Ribo-seq

2 uncovered 37 translated sORF candidates that were novel compared to both in GenBank

3 2014 and RefSeq 2017 annotations (**Table S7**).

4
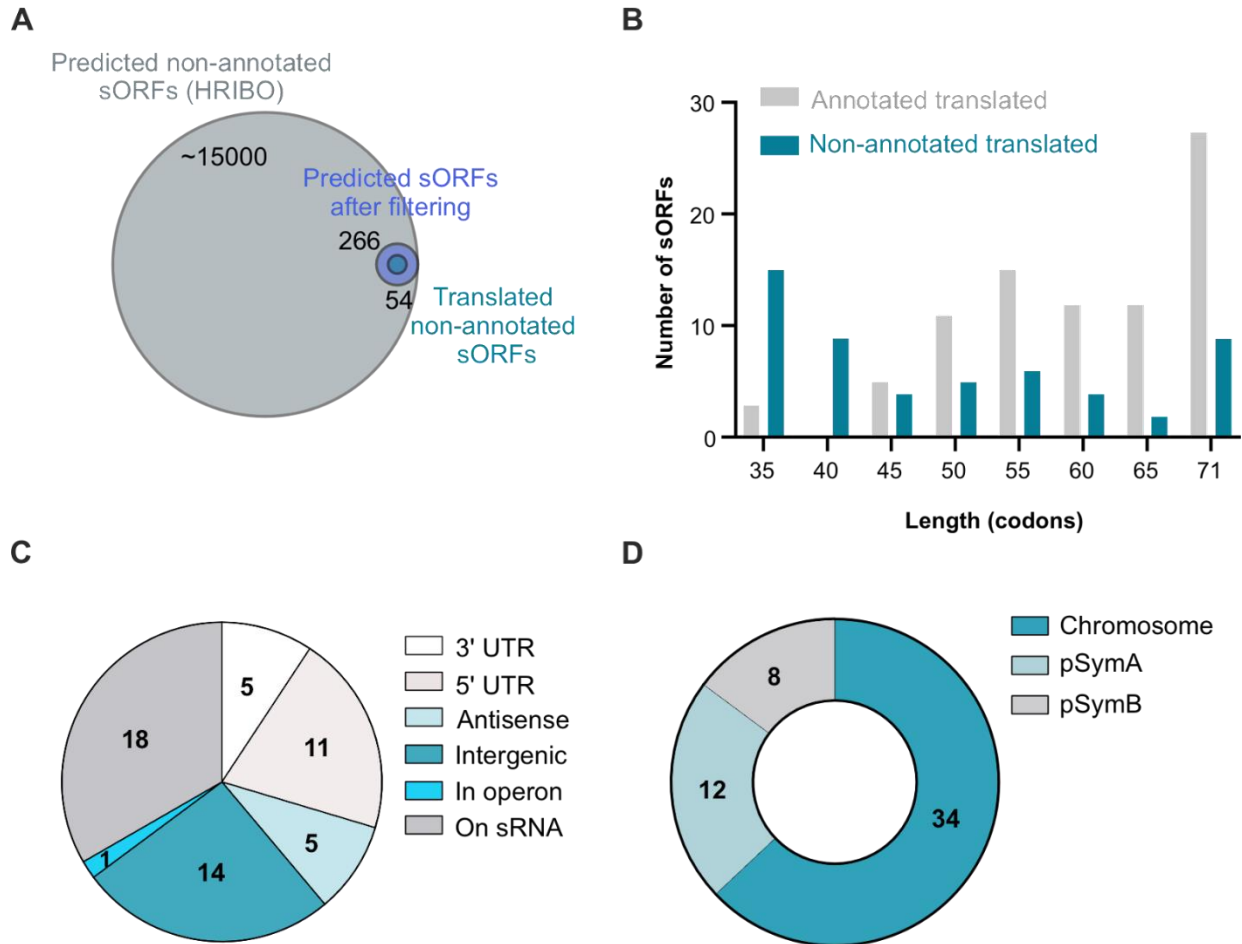
5

6 **Figure 4. Ribo-seq uncovers a repertoire of small open reading frames (sORFs) missing**

7 **from the *Sinorhizobium meliloti* 2011 genome annotation. (A)** sORF predictions from HRIBO

8 included a high number of potential non-annotated sORFs (approximately 15,000). These sORFs

9 were first filtered (TE of ≥ 0.5, RNA-seq and Ribo-seq RPKM of ≥ 10, DeepRibo score of > −0.5)

10 to generate a set of 266 translated sORF candidates that were additionally manually curated by

11 inspection of the Ribo-seq read coverage in a genome browser. Overall, 54 high-confidence non-

12 annotated sORFs displayed active translation during growth in minimal medium. A Venn diagram

13 shows the respective number of proteins from each category (scaled with area size). Diagrams

14 were prepared with BioVenn (www.biovenn.nl). **(B)** Histogram showing the length distribution

15 of the 54 non-annotated versus the 85 annotated sORFs identified as translated by Ribo-seq. **(C)**

16 Genomic context of the translated non-annotated sORFs. **(D)** Replicon distribution of the

17 translated non-annotated sORFs.

18

1   **Both standard and small custom iPtgxDBs informed by Ribo-seq data facilitate novel**

2   **SEP identification by MS**

3   To validate sORF translation and identify novel SEPs of *S. meliloti* 2011, we then conducted

4   MS-based proteomics using experimental strategies to increase the coverage of the MS-

5   detectable small proteome and two search DBs. Cells were cultured either in minimal GMS

6   medium (same as for Ribo-seq) or in rich TY medium, and three complementary sample

7   preparation approaches were used: 1) tryptic in-solution digest of all proteins (a standard

8   proteomics approach), 2) solid phase enrichment (SPE) of small proteins with subsequent

9   Lys-C digestion, and 3) SPE of small proteins without subsequent digestion (**Fig. 5A**).

10 Approaches 2 and 3 can identify SEPs whose peptides are not within the detectable range

11 (approximately 7 aa to 40 aa) upon a tryptic digest (Tyanova et al. 2016).

12 For the DB searches, we first relied on a standard (full) iPtgxDB (Omasits et al. 2017) that

13 hierarchically integrates reference genome annotations, *ab initio* gene predictions, and *in*

14 *silico* ORF predictions (see **Methods**). The overlap and differences of all annotation sources

15 were captured and consolidated in a composite gene identifier. Moreover, a large but

16 minimally   redundant   protein   search   DB   (for   more   details,   see

17 https://iptgxdb.expasy.org/creating iptgxdbs/) is created, as well as a GFF that allows

18 researchers to overlay experimental evidence, such as RNA-seq, Ribo-seq, or proteomics data.

19 Individual iPtgxDBs must be prepared for different proteases (see **Methods**). For trypsin, the

20 standard iPtgxDB contained close to 160k protein entries of approximately 103k annotation

21 clusters (**Table S3.1**), that is, genomic loci that share the stop codon but have different

22 predicted protein start sites. Approximately 92% of the peptides unambiguously identify one

23 protein entry, which are called class 1a peptides that facilitate downstream data analysis and

24 allow to swiftly identify novel proteoforms or SEPs. Although standard iPtgxDBs are very

25 large, when combined with stringent FDR filtering, they have provided convincing results in

26 the past, that is, for the identification of novel SEPs that withstood independent validation

27 efforts (Omasits et al. 2017; Melior et al. 2020; Bartel et al. 2020). However, as large DBs

28 inflate the search space, they complicate protein inference and FDR estimation, resulting in a

29 large likelihood of a random hit, especially for SEPs (Fancello and Burger 2022; Nesvizhskii

30 2010). Importantly, the 266 top Ribo-seq-implied novel candidates (**Fig. 4A**) allowed us to

31 explore whether a much smaller custom iPtgxDB may provide additional value for the

32 identification of annotated or novel SEPs. Adding these 266 candidates to the three reference

1   genome annotations (RefSeq, GenBank, Genoscope) and the Prodigal *ab initio* gene

2   predictions resulted in a 20-fold smaller custom iPtgxDB (**Fig. 5A**) (approximately 8,000

3   protein entries in 7,300 annotation clusters), with a higher percentage of class 1a peptides

4   (nearly 98%; **Table S3.3**).
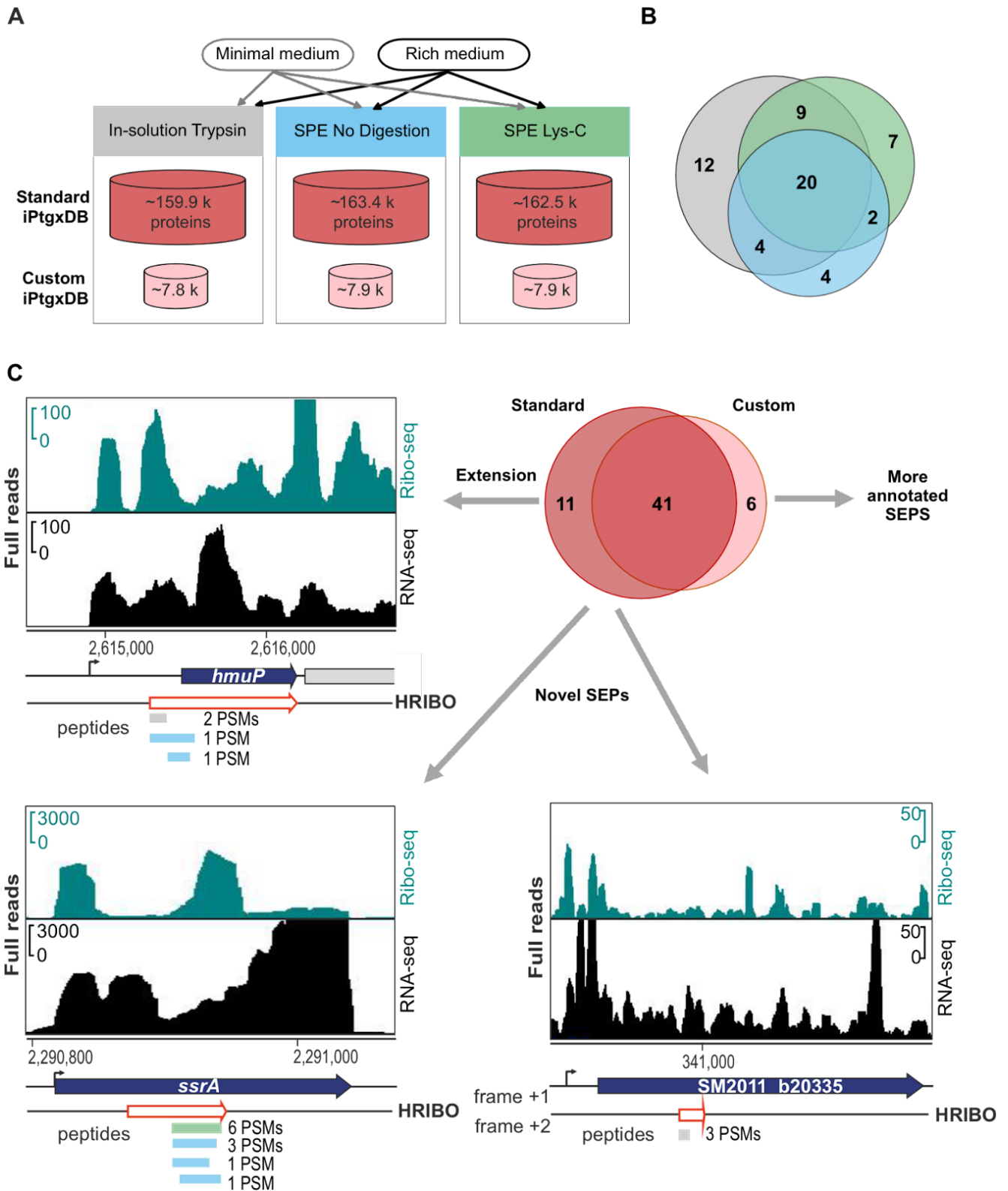
5

1 **Figure 5**. **Mass spectrometry-based identification of known and novel small open reading**
2 **frame-encoded proteins (SEPs). (A)** Experimental set-up for the proteomics analyses. Bacteria
3 were grown in minimal and rich media, and protein extracts were further processed with tryptic in-
4 solution digest (gray), solid-phase enrichment (SPE) of small proteins with subsequent Lys-C
5 digestion (green), or without further digestion (blue). **(B)** Overlap of the identified SEPs by
6 experimental approach; trypsin identified 45 SEPs; compared with the trypsin approach, Lys-C
7 identified 38 SEPs (nine novel, 24%), and the approach without digestion found 30 SEPs (six novel,
8 20%). **(C)** Novel/unique identifications uncovered by the standard integrated proteogenomic search
9 databases (iPtgxDB) and the small custom iPtgxDB. Standard iPtgxDB: Three peptides imply a 14 aa
10 longer proteoform (60 aa) for HmuP than annotated; four peptides of the tmRNA-encoded proteolysis
11 tag were identified; one peptide (3 peptide spectrum matches [PSMs]) implied a novel SEP (34 aa)
12 internal to the genomic region that also encodes SM2011_b20335 but in a different frame. Spectra
13 identifying these peptides are shown in **Fig. S5**. These identifications were also predicted by HRIBO
14 based on Ribo-seq. Finally, six annotated proteins (GenBank 2014 and/or RefSeq 2017) were
15 identified only in the search against the small custom iPtgxDB, as they did not accumulate enough
16 spectral evidence in the search against the standard iPtgxDB (**Table S4**).

17

18 The acquired MS-spectra were searched against the standard and small iPtgxDBs, and the
19 results were compiled and stringently filtered, requiring more PSM evidence (see Methods)
20 for *ab initio* and *in silico* predictions (Varadarajan et al. 2020a; Varadarajan et al. 2020b).
21 Overall, more than 1,200 annotated proteins were detected at an estimated protein FDR of
22 approximately 1%. The SPE-based small protein enrichment steps uniquely identified 160 of
23 these proteins (**Fig. S4A**). Notably, the search against the small custom DB accounted for 112
24 unique identifications (**Fig. S4B**), presumably due to improved search statistics. The MS-
25 identified proteins included 58 SEPs, with ≤ 70 aa, 47 of which were annotated (GenBank
26 2014 and/or Refseq 2017) (**Table S4**). Similar to the overall results, the two SPE approaches
27 also added unique SEPs: while 45 of the 58 MS-detected SEPs were identified with standard
28 trypsin-based digestion, 13 SEPs were uniquely identified after processing the samples with
29 SPE and either a Lys-C digest (9 of 38 not covered by trypsin) or no proteolytic digest (6 of
30 30 not covered by trypsin) (**Fig. 5B**). Most MS-identified SEPs were between 60 and 70 aa
31 long (67%), and the smallest detected SEP was 20 aa long. They include abundantly expressed
32 proteins (the cold shock proteins RS25125 and RS00515, and RS31025, a 50S ribosomal
33 protein L32) (**Table S4**) down to candidates identified by only 2 PSMs, such as a 59 aa
34 hypothetical protein, which we refer to as SEP7 (see next section). Among the 85 GenBank-

1   annotated SEPs identified with high confidence, as translated by Ribo-seq (**Fig. 3A**), 31 were

2   identified by MS. Among the 54 SEPs missing from the GenBank annotation and identified as

3   translated by Ribo-seq (**Fig. 4A**), five were identified by MS, and those are present in the

4   Refseq 2017 annotation (**Table S4**).

5   Importantly, both searches added unique identifications. The search versus the full iPtgxDB

6   added 11 potential novel SEPs or longer proteoforms than annotated, which were *in silico*

7   predictions that were excluded from the small custom iPtgxDB. A 14 aa longer proteoform of

8   HmuP was identified by three peptides with 4 PSMs (**Fig. S5A**). Here, when manually

9   inspecting the Ribo-seq data, it perfectly agreed with the extension of the 46 aa GenBank

10   annotation (**Fig. 5C**). This finding exemplifies how proteomics and Ribo-seq jointly identify a

11   novel proteoform. Furthermore, the tmRNA-encoded 12 aa proteolysis tag peptide was

12   uniquely identified, which marks incompletely translated proteins for degradation (Karzai et

13   al. 2000) (**Fig. 5C**). The tag peptide was identified as a C-terminal part of an *in silico* predicted

14   23 aa SEP included in the standard iPtgxDB. It was only detected in the minimal medium by

15   four peptides: one in the Lys-C digest and three from the search without protease (**Fig. 5C**

16   and **S5B**). Mutation of the start codon of the 23 aa sORF had no effect on the translation of the

17   proteolysis tag peptide, in line with the mechanism proposed for this split tmRNA (Ulvé et al.

18   2007; Keiler et al. 2000) (**Fig. S6**). An example of a completely novel 34 aa SEP is shown in

19   the third panel of **Fig. 5C** (see also **Fig. S5C**); it is located in a genomic region that harbors an

20   annotated CDS and is translated in a different frame. The novel sORF has Ribo-seq support

21   (TE 0.4) but did not pass our stringent Ribo-seq cut-offs. Notably, the search against the small

22   custom iPtgxDB added six unique SEP identifications (again, due to better search statistics)

23   (**Fig. 5C**). Four of them were also among the 85 GenBank-annotated SEPs identified by Ribo-

24   seq data (RS33030, RS33620, RS33980, and a6027), lending independent support for their

25   expression (**Table S4**). RS33620 belongs to the arginine-rich DUF1127 family of proteins, the

26   members of which are involved in phosphate and carbon metabolism in *Agrobacterium*

27   *tumefaciens* (Kraus et al. 2020), and in RNA maturation and turnover in *Rhodobacter*

28   (Grützner et al. 2021). In addition, the abovementioned RefSeq-annotated SEP7 was

29   identified (**Fig. S5D**). Two other SEPs (one of them novel) were identified with only 1 PSM

30   (**Fig. S5E** and **S5F**), which was below our threshold, but had strong Ribo-seq support (SEP1,

31   SEP20; see next section).

32

**Validation of a subset of Ribo-seq-implied small proteins by Western blot analysis**

Since out of the 54 high-confidence Ribo-seq-implied sORFs that were not contained in the GenBank annotation (2014) only five were detected with at least 2 PSMs in the MS analysis (**Table S4**), we attempted validation by epitope tagging and Western blot analysis (**Fig. 6**). Nineteen sORFs were selected that i) cover a broad range of TE values, ii) start with one of the three main start codons (ATG: 16 sORFs, GTG: two sORFs, or TTG: one sORF), and iii) were either added in the RefSeq 2017 annotation (five sORFs) or were novel with respect to these two annotations (14 sORFs). The corresponding proteins were designated SEP1 to SEP19 (**Table S4**). They included three of the candidates that were also detected by MS (SEP7: 2 PSMs; SEP 10: 59 PSMs; SEP17: 29 PSMs). SEP1 was only identified by 1 PSM, that is, below the threshold (**Table S4; Fig. S5E**), but with strong Ribo-seq support (highest TE among the 54 high-confidence Ribo-seq candidates; **Table S7**). Moreover, three SEP candidates below 30 aa (SEP1, SEP3, and SEP6) and four candidates with a predicted transmembrane helix (TMH) (SEP4, SEP6, SEP13, and SEP16; **Table S4**) were analyzed. As a 20th candidate (SEP20), we included a conserved annotated sORF located in the cytochrome C oxidase cluster *ctaCDBGE* between *ctaB* and *ctaG* (GenBank annotation 2014), which also contains a predicted TMH. SEP20 was identified by 1 PSM in the MS analysis (**Fig. S5F**) and did not pass the stringent HRIBO criteria for translated candidate sORFs (**Table S3,** TE = 6.99, RPKM of < 10 in replicate 1) but showed strong read coverage in the Ribo-seq library (**Table S6**).

Each sORF was cloned together with its −15 nt 5′ UTR region, thus containing its putative ribosome binding site in frame to the SPA-tag encoding sequence into plasmid pSW2 (**Fig. 6A** and **Fig. S1**). Transcription of the sORF::*spa* fusion is under the control of a *S. meliloti sinI* promoter (P$_{sinI}$) of moderate strength, which is constitutively active (Charoenpanich et al. 2013). Thus, the detection of a SEP-SPA fusion protein by Western blot analysis would indicate sORF translation. The Western blot analysis of crude lysates of cultures grown in minimal medium using FLAG-directed antibodies revealed signals for 15 of the 20 candidates, including SEP20 (see **Fig. 6B–6G**). For the 12 candidates, one band consistent with their predicted SEP length was detected. For SEP1 and SEP5, on top of the expected SEP-SPA bands, slow migrating bands at approximately 25 kDa (see asterisks in **Fig. 6E**) were detected, which probably corresponded to a non-specific signal, as they were also detected in some EVC samples after lysate fractionation (**Fig. S7**).
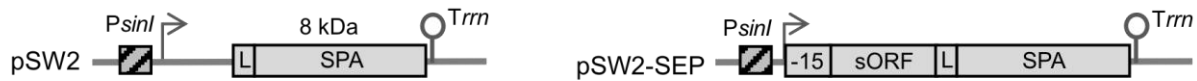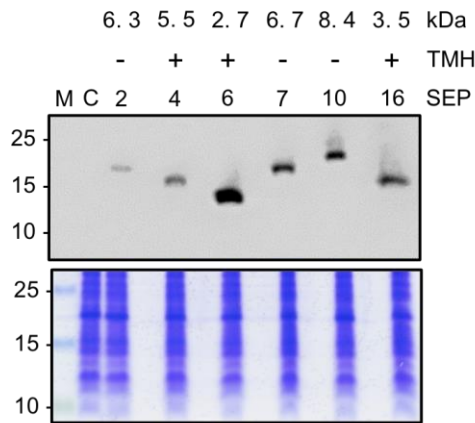
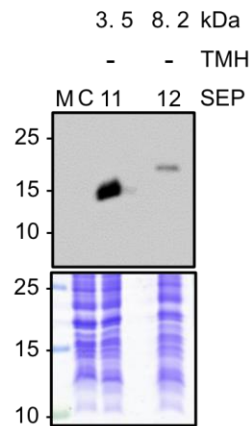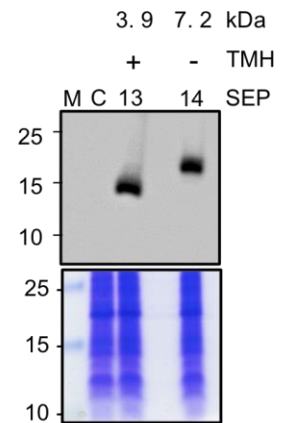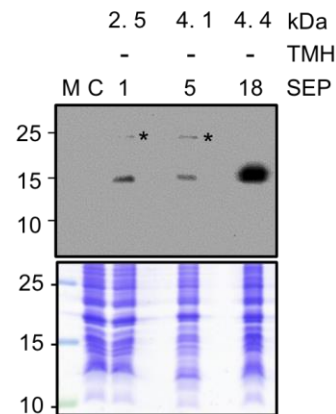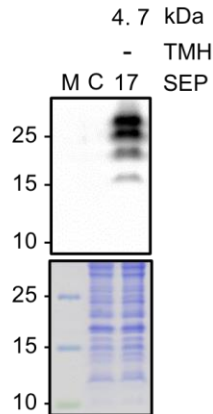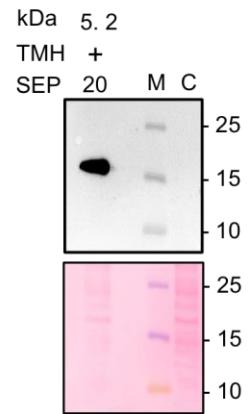**Figure 6**. **Detection of 15 sequential peptide affinity (SPA)-tagged small open reading frame-encoded proteins (SEPs) in *Sinorhizobium meliloti* crude lysates. (A)** Schematic representation of the empty plasmid pSW2 (contains no promoter and no ribosome-binding site upstream of the linker [L] and SPA-encoding sequence) and a pSW2-SEP plasmid for the analysis of sORF translation. The constitutive P*sinI* promoter (hatched box), the corresponding TSS (flexed arrow), the sORF coding sequence with its −15-nt-long region, the SPA-tag (with its molecular size indicated) preceded by a linker (L) (gray boxes), and the T*rrn* terminator (hairpin) are depicted. **(B) to (F)** Western blot analysis of crude lysates (upper panels) and the corresponding Coomassie-stained gels, and **(G)** corresponding Ponceau-stained membrane for selected SEPs. Monoclonal FLAG-directed antibodies were used. Migration of marker proteins (in kDa) is shown on the left side. * Unspecific signal. Above the panels, the numbers of the analyzed SEP protein (see **Table S7**), the presence (+) or absence (−) of a predicted TMH, and the molecular size (in

31

1   kDa) of the SEP without the SPA tag are given. M: protein marker. C: empty vector control, lysate

2   from a strain containing pSW2.

3

4   The bands of the tagged SEP1 and SEP5 ran similarly, although SEP1 is smaller than SEP5,

5   as indicated above the panel (**Fig. 6E**). Probably, the aberrant migration of SEP1 is due to

6   its acidic aa composition (pI of 4.18) (Guan et al. 2015). SEP17 showed multiple bands,

7   with a weak and fast migrating band at approximately 15 kDa, which probably

8   corresponds to the monomeric SEP17-SPA protein, and three strong and slow migrating

9   bands, which could indicate protein oligomerization (**Fig. 6F**). Overall, the translation of

10   SEPs with alternative start codons, that is, GTG (SEP10 and SEP14) and TTG (SEP7), and

11   of the five candidates missed in the GenBank (2014) annotation but included by Refseq

12   (2017) (SEPs Nr. 4, 7, 10, 17, and 18), was validated. Importantly, this analysis confirmed

13   the translation of six novel SEPs (SEPs Nr. 1, 6, 11, 13, 14, and 16), including two of the

14   three SEP candidates shorter than 30 aa. Finally, our observation that 11 (out of 16) sORFs

15   without MS support but with high confidence Ribo-seq data were validated in the Western

16   blot analysis shows the power of Ribo-seq to detect novel translated sORFs.

17   Since the analysis of exclusive or predominant subcellular localization is valuable for

18   linking hypothetical proteins without any annotation to some potential function

19   (Stekhoven et al. 2014), we decided to investigate the subcellular localization of the

20   validated SPA-tagged SEPs by Western blot analysis of the supernatant (S100) and pellet

21   (P100) fractions (see Methods) (**Fig. S7**). As expected, the predicted TMH-containing

22   proteins SEP4, SEP6, SEP13, SEP16, and SEP20 were detected exclusively or

23   predominantly in P100, which contains ribosomes and membranes, whereas the

24   predicted cytoplasmic proteins SEP5 and SEP12 were detected exclusively in the S100

25   fraction (**Fig. S7**). The remaining eight SEPs were detected exclusively or partially in the

26   P100 fraction, suggesting that they could be associated with membrane complexes or

27   ribosomes (SEP10 and SEP18 show similarities to the ribosomal proteins S21 and L7/12)

28   or be prone to aggregation in their recombinant, tagged form.

29

30

Conservation and potential functions of *S. meliloti* novel small proteins

As described above, we detected the translation of 48 sORFs missing in the GenBank 2014 and Refseq 2017 annotations (37 identified by Ribo-seq and additional 11 by MS), which we refer to as novel. Since conserved SEPs are likely to be functional, we used tBLASTn (Gertz et al. 2006) to examine the conservation of the proteins encoded by the 48 novel sORFs (**Fig. 7; Table S8**). The tBLASTn searches were conducted in bacteria with parameters previously established to identify conserved bacterial sORFs (Allen et al. 2014) (see **Methods**). We found a wide range of conservation, from an sORF detected in only four *S. meliloti* strains overall, to sORFs conserved at different higher taxonomic levels, to highly conserved sORFs present in different bacterial phyla (**Fig. 7**). Among the 14 sORFs encoding SEPs with < 30 aa (excluding the tmRNA sORF64), four are conserved beyond *S. meliloti*. One of the most widely conserved novel SEPs is a 64-aa-long small protein detected only by MS (sORF61 in **Fig. 7**). It was identified as a product of an *in silico* predicted sORF, with 3 PSMs in lysates from MM cultures (**Fig. S5G; Table S4**). However, no expression at the level of RNA was detected at its locus, possibly suggesting high protein stability. sORF61 has homologs in several bacterial phyla and multiple paralogs, with a maximal aa sequence identity of 64% on each replicon in *S. meliloti* 2011. Despite its wide distribution and strong conservation, its function is unknown. Overall, excluding the tmRNA, we detected seven sORFs conserved beyond the family *Rhizobiaceae,* suggesting that the corresponding SEPs may have important general functions.

Furthermore, we used TMHMM (Krogh et al. 2001) and PSORTb (Yu et al. 2010) to predict the presence of transmembrane helices and the subcellular localization of the 48 novel SEPs. Localization in the cytoplasmic membrane was predicted for seven SEPs using at least one of the tools (**Fig. 7; Table S8**). Among them are the Ribo-seq-identified and Western blot analysis-validated SEP6 (prediction by both TMHMM and PSORTb) and SEP16 (prediction by TMHMM only), which were detected with strong signals predominantly in the P100 fraction (see **Fig. S7**). The corresponding sORF6 and sORF16 are conserved in *Hyphomicrobiales* (**Fig. 7**). No proteins with predicted membrane localization were found among the 11 MS-detected SEPs (**Fig. 7**). Notably, two of the 48 novel SEPs harbor a predicted SpII cleavage site and are thus probably lipoproteins (**Fig. 7**). Lipoproteins play important roles in physiology, signaling, cell envelope structure, virulence, and antibiotic resistance (Kovacs-Simon et al. 2011); however, as we had

1 previously reported, they are often missed in prokaryotic genome annotations (Omasits

2 et al. 2017).

3
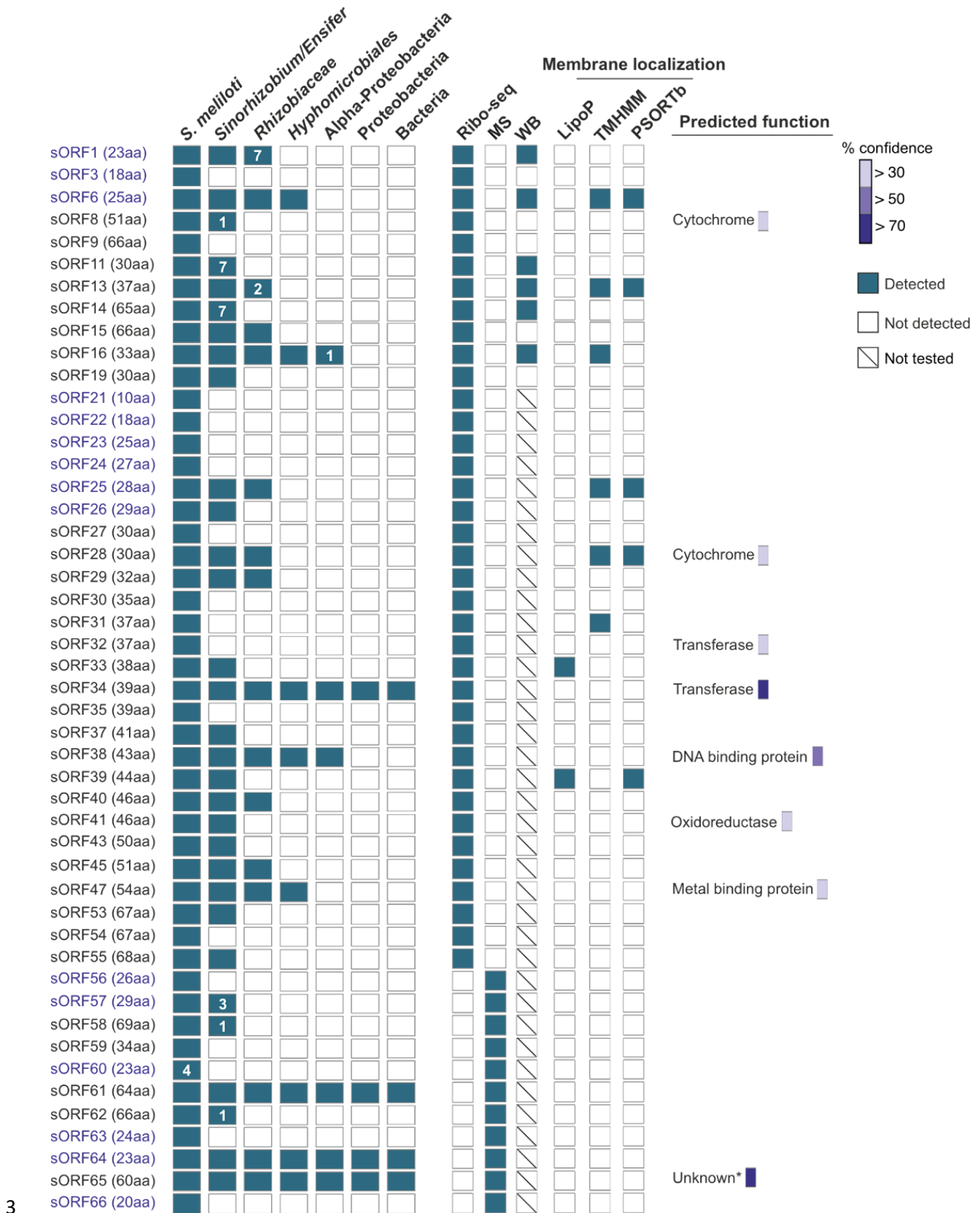
Figure 7. Conservation analysis and functional prediction for 48 novel small open reading frames (sORFs) of *Sinorhizobium meliloti* 2011. The conservation analysis was conducted using tBLASTn. The respective hits (see methods for parameters and cutoffs) are broadly summarized at the level of different taxonomic groups. The number of species outside the lower taxonomic unit, which harbors a hit, is given, if at < 10. In addition, the method by which the respective sORF was detected or confirmed is shown (Ribo-seq: ribosome profiling, MS: proteomics, WB: Western blot), as well as the results of predictions for membrane localization (by TMHMM and PSORTb), signal peptide II cleavage sites of lipoproteins (by LipoP), and function (by Phyre2; only hits with confidence levels greater than 30% are shown). sORF1 to sORF55 are a subset of the 57 Ribo-seq-detected, translated sORFs, which are listed in Table S7, and sORF56 to sORF66 represent the novel sORFs identified by proteomics. sORFs encoding small proteins below 30 amino acids are shown in blue. The putative sORF64, present in tmRNA, contains the proteolytic tag sequence. The sORF65 corresponds to the N-terminal HmuP extension; outside of Proteobacteria, it is conserved in many genera of Planctomycetes. *Structural genomics (92% confidence homology to protein of unknown function).

Moreover, we used Phyre2 (Kelley et al. 2015) to gain insights into the potential functions of novel SEPs with ≥ 30 aa by analyzing their similarity to proteins with known tertiary structures (**Fig. 7; Table S8**). Best hits with a confidence homology of ≥ 30% were obtained for eight novel SEPs (**Fig. 7**). The highest confidence homology suggesting a function was obtained for the SEPs encoded by sORF38 (DNA binding; 18 of the 43 aa residues were modeled with 66% confidence homology; conserved in Alphaproteobacteria) and sORF34 (bleomycin resistance; 37 of the 39 aa residues were modeled with 92% confidence homology; conserved among Bacteria). The HmuP extension (sORF65 in **Fig. 7**; see also **Fig. 5C**) was modeled with 98% confidence along 59 of its 60 aa residues; however, according to Phyre2, the function of the hit was unknown. Overall, obtaining clear functional predictions was not possible even for conserved SEPs, most probably due to their small size.

We also suggest the functions for three annotated sORFs/SEPs with validated translation. SEP5 (added in the RefSeq 2017 annotation) is conserved only in *Sinorhizobium*. Its translation was detected with Ribo-seq and Western blot analysis (**Fig. 6E; Table S4**). The SEP5 sORF contains a cluster of six threonine and three lysine codons near its 3′ ′end and is located in the 5′ UTR of the aspartate dehydrogenase-encoding gene. Since aspartate is a part of the threonine and lysine biosynthesis pathway (Vitreschak et al.

1   2004), our observation suggests that this sORF can be involved in the post-transcriptional

2   regulation of the aspartate dehydrogenase gene in *Sinorhizobium*, and SEP5 is possibly a

3   leader peptide*.* Furthermore, among the annotated SEPs with functional assignment,

4   which were detected by MS, an entericidin A/B family lipoprotein was found

5   (CP004140.1:2141558-2141716:-, **Table S4**). The 52-aa-long protein has a predicted

6   TMH and is conserved in Alphaproteobacteria. Its *A. tumefaciens* homolog, the lipoprotein

7   Atu8019, is involved in specific cell–cell interactions as a part of outer membrane vesicles

8   (Knoke et al. 2020). Finally, an annotated small protein validated in this work by Ribo-

9   seq and Western blot analysis (1 PSM in the MS) is the abovementioned SEP20 (**Fig. 6G,**

10   **Fig. S5E; Table S4**). It contains a predicted TMH and is conserved in the

11   Alphaproteobacteria, and its sORF is part of an uncharacterized cytochrome oxidase

12   operon. This synteny suggests that SEP20 can participate in the assembly and/or function

13   of the corresponding cytochrome oxidase complex, as previously shown for SEP CydX and

14   cytochrome bd oxidase in *Brucella abortus* (Sun et al. 2012).

15

16   **DISCUSSION**

17   In this work, we have developed and applied a Ribo-seq workflow to comprehensively map

18   the translatome of *S. meliloti* 2011 under free-living conditions in a minimal medium. By

19   combining Ribo-seq and MS-based proteomics in a proteogenomic approach, we added 48

20   novel SEPs with nearly 70 aa to the *S. meliloti* annotation, that is, an increase in the number

21   of annotated SEPs (present in at least one of the GenBank 2014 and RefSeq 2017 annotations)

22   by approximately 17%.

23   Ribo-seq is a powerful technique for detecting translation on a global scale with high

24   sensitivity (Ingolia et al. 2019). However, in contrast to eukaryotic model systems, codon

25   resolution has not yet been achieved in Ribo-seq analyses of bacteria (Cianciulli Sesso et al.

26   2021; Mohammad et al. 2019; Vazquez-Laslop et al. 2022; Venturini et al. 2020). Trapping

27   ribosomes on mRNA and generating ribosome footprints have remained challenging,

28   requiring careful optimization for each bacterial species. Our Ribo-seq workflow for *S.*

29   *meliloti* includes ribosome trapping by rapid cooling of the culture without using antibiotics

30   and cell lysis in an adapted buffer, followed by digestion of unprotected RNA by RNase I,

31   which is not inactivated by the ribosomes of *S. meliloti* (**Fig. 1B**). RNase I has the advantage

32   of precisely cleaving at both 5′ and 3′ ends of ribosome-protected mRNA without sequence

1 specificity, in contrast to the routinely used MNase (Bartholomäus et al. 2016). The digestion

2 of 5′ and 3′ regions of translated mRNAs (**Fig. 1C, Fig. 3C**), higher TEs of annotated CDS in

3 comparison to non-coding RNAs (**Fig. 2B**), and pronounced ribosome protection up to 16 nt

4 upstream and downstream of start codons (**Fig. S2; Fig. 1C** and **1D**) show the successful

5 establishment of Ribo-seq for *S. meliloti.*

6 In addition to providing the first genome-wide ribosome-binding map of a *Hyphomicrobiales*

7 member, our Ribo-seq analysis uncovered translation for 85 annotated sORFs and identified

8 37 novel sORFs missing in the GenBank 2014 and Refseq 2017 annotations of the *S. meliloti*

9 genome. The translated sORFs were found on all three replicons and had similar preferences

10 for start and stop codons independently of whether they were annotated or novel (**Fig. 3** and

11 **Fig. 4**). The novel sORFs were generally shorter than the annotated ones (**Fig. 4B; Table S4**),

12 clearly showing the advantage of the Ribo-seq method for SEP discovery. Many of the novel

13 sORFs were probably not annotated due to their location in short transcripts considered as

14 non-coding RNAs or asRNAs or in 5′ and 3′ UTRs (**Fig. 4C**).

15 Several translated novel sORFs internal to annotated genes (nested ORFs; Gray et al. 2022)

16 were also predicted by our Ribo-seq data. However, they were excluded from the analysis as

17 additional evidence is needed to confirm their existence. Targeted detection of translation

18 initiation sites is useful in uncovering such sORFs by Ribo-seq (Meydan et al. 2019; Weaver

19 et al. 2019), a strategy beyond the scope of our study. However, the existence of an internal

20 sORF predicted by Ribo-seq was supported by the MS detection of a novel, 34-aa-long SEP

21 translated in a different frame in the genomic region encoding SM2011_b20335 (**Fig. 5C** and

22 **Fig. S5G;** sORF59 in **Fig. 7**).

23 A challenge in defining novel sORFs for any genome is that annotations from different

24 reference genome annotation centers can differ substantially for an identical sequence and

25 change over time; that is, CDS are being added but are also removed in more recent

26 annotations (see **Fig. 2F** and the "master" **Table S4**). Accordingly, two of the 48 novel SEPs

27 are now bona fide-predicted CDS in the latest RefSeq 2022 annotation, with MS-evidence of

28 a single PSM found with the custom iPtgxDB, whereas two other Ribo-seq-identified sORFs

29 have variable pseudogene status in different annotation releases (see **Table S4**). iPtgxDBs,

30 which integrate existing reference annotations and add *in silico* predicted ORFs in all six

31 frames to virtually cover the entire protein coding potential of a prokaryote, can be used to

32 overcome such problems and enable MS-based detection of novel SEPs (Omasits et al. 2017).

1   Here, in addition to a standard large iPtgxDB of *S. meliloti* (Melior et al. 2020), we applied the
2   concept of a small, custom iPtgxDB lacking *in silico* predictions and including the top
3   predictions from our experimental Ribo-seq data. This custom iPtgxDB is approximately 20-
4   fold smaller and benefits statistics and FDR estimation (Li et al. 2016; Blakeley et al. 2012).
5   Notably, although the identification of 11 *in silico* predicted novel sORFs was possible only
6   with the standard iPtgxDB, the small iPtxDB contributed substantially to the validation of
7   annotated sORFs, increasing the number of SEPs with experimental support by 10% (**Fig. S4**).
8   The detection of more SEPs was also facilitated by applying three experimental approaches,
9   two of which included enrichment of small proteins. The MS detection of enriched SEPs
10   without a proteolytic digest, including, for example, the 12 aa proteolysis tag encoded by
11   tmRNA (**Fig. 5C** and **Fig. S5**), shows that this method can be useful for the identification of
12   SEPs.

13   The validation of translation by Western blot analysis for 15 out of 20 analyzed novel SEPs
14   with Ribo-seq support (**Fig. 6B–6F; Table S7**), only three of which were detected by MS with
15   at least 2 PSMs (**Table S4**), underlines the power of the Ribo-seq technique for identification
16   of translated sORFs. The example of SEP7 (**Fig. 6B**; 59 aa, restriction endonuclease-like,
17   conserved in *Rhizobiaceae*), which was added to the RefSeq annotation 2017 and was
18   detected by 2 PSMs using the small, custom iPtgxDB, illustrates the added value of the latter.
19   Detection of translation for the novel SEP1 (23 aa, conserved in *Rhizobiaceae*) by Western
20   blot analysis (**Fig. 6E**) and Ribo-seq (highest TE among the non-annotated translated sORFs,
21   **Table S7**), even though it was identified by only 1 PSM in the MS analysis (**Fig. S5E**), suggests
22   that putative SEPs with 1 PSM can be truly expressed, real small proteins. Similarly, the
23   annotated SEP20 (46 aa, conserved in Alphaproteobacteria) was confirmed by Western blot
24   analysis (**Fig. 6G**), although it had only 1 PSM (**Fig. S5F**) and did not pass the stringent manual
25   evaluation of the Ribo-seq data (**Table S7**). We suggest that the conservation analysis of
26   putative SEPs, which have minimal MS evidence (e.g., 1 PSM) and/or correspond to sORFs
27   that did not pass the very stringent manual curation of the Ribo-seq data, can help define SEP
28   candidates with potentially important functions that can be validated and analyzed in the
29   future.

30   Despite the lower sensitivity of MS compared with Ribo-seq, using MS we detected 16
31   additional SEPs that were not identified as translated by Ribo-seq. Eleven of them were novel,
32   showing the importance of complementary methods for comprehensive analysis of bacterial

38

1 small proteomes. The reported numbers of validated and novel sORFs and their encoded SEPs

2 are affected by the somewhat arbitrary cut-off of 70 aa. In fact, our data provide evidence for

3 the translation of three additional, non-annotated proteins below 100 aa, which are

4 considered small in other studies (Baumgartner et al. 2016; Kaulich et al. 2021; VanOrsdel et

5 al. 2018) (see **Table S4**).

6 The functions of small proteins are difficult to predict *in silico*, often because they are too

7 small to harbor known protein domains or motifs (Ahrens et al. 2022). In addition, for SEPs

8 smaller than 30 aa *in silico* analysis by Phyre2 is still impossible. Keeping these limitations

9 in mind, we present a list of putative functions corresponding to Phyre2 best hits (**Table**

10 **S8**). Since modeling of a partial SEP sequence by Phyre2 may provide a hint of potential

11 interactions with other proteins or protein complexes, we mention predictions based on

12 greater than 30% confidence homology in **Fig. 7,** including the predicted DNA-binding

13 function of the 43 aa SEP38 and a potential role in bleomycin resistance of the 39 aa SEP34.

14 SEP function can also be predicted based on gene synteny (Ahrens et al. 2022), as

15 mentioned above, for SEP5 (potential leader peptide encoded by a regulatory upstream

16 sORF) and SEP20 encoded in a cytochrome oxidase operon. Our findings show that,

17 excluding the tmRNA sORF, 13 out of the 48 novel SEPs (sORFs) are conserved in

18 *Rhizobiaceae*, seven in *Hyphomicrobiales*, and three in at least two bacterial phyla, which

19 likely suggests physiological relevance. Most of the translated sORFs or SEPs were detected

20 in logarithmic cultures grown in a minimal medium, where bacteria synthesize virtually all

21 metabolites for cell reproduction. Thus, some of these SEPs can be of general importance

22 for growth or are needed for survival and competitiveness under oligotrophic conditions in

23 soil and rhizosphere.

24 In summary, our work shows that a combination of methods is beneficial for increasing the

25 number of experimentally validated SEPs. Using Ribo-seq, MS, and Western blot analysis of

26 C-terminally tagged proteins, we provide evidence for the translation of 48 SEPs with ≤ 70 aa

27 to be added to the annotation of *S. meliloti*, thus substantially increasing the number of

28 cataloged SEPs. With the MS data, the corresponding full and small custom iPtgxDBs, and

29 importantly, the first Ribo-seq analysis of a *Hyphomicrobiales* member, which can be viewed

30 with an interactive online JBrowse instance (http://www.bioinf.uni-freiburg.de/ribobase),

31 our study provides valuable resources for future studies on and beyond the small proteome.

ACKNOWLEDGEMENTS

CONFLICT OF INTEREST

The authors declare that they have no conflicts of interest.

AUTHOR CONTRIBUTIONS

CMS, RB, and EEH initiated the project. LH, RG, SM, RS, SA, CHA, BH, and EEH designed the experiments and analyzed the data. LH established Ribo-seq for *S. meliloti,* performed the Ribo-seq analysis, manually examined the implied novel sORFs, explored evolutionary conservation, and predicted the function of novel SEPs. RG performed the bioinformatic processing of the Ribo-seq data. SM conducted the mass-spectrometry experiments, database searches and manually evaluated spectra implying novel SEPs. BH and CHA contributed to the proteogenomic analysis to identify the known and novel SEPs, explored the value of iPtgxDBs for Ribo-seq data, consolidated experimental results in a master table, and identified annotation differences. RS, SA, and SBW performed the cloning and Western blot analyses. LH, CHA, and EEH mainly wrote the manuscript with input and feedback from the other authors. DB, RB, CMS, CHA, and EEH supervised the research and provided resources and funding. All authors approved the submitted version.

REFERENCES

Ahrens CH, Wade JT, Champion MM, Langer JD. 2022. A practical guide to small protein discovery and characterization using mass spectrometry. *J Bacteriol* **204**: e0035321.

Allen RJ, Brenner EP, VanOrsdel CE, Hobson JJ, Hearn DJ, Hemm MR. 2014. Conservation analysis of the CydX protein yields insights into small protein identification and evolution. *BMC Genomics* **15**: 946.

Aoyama JJ, Raina M, Zhong A, Storz G. 2022. Dual-function Spot 42 RNA encodes a 15-amino acid protein that regulates the CRP transcription factor. *Proc Natl Acad Sci USA* **119**: e2119866119.

Barra-Bily L, Fontenelle C, Jan G, Flechard M, Trautwetter A, Pandey SP, Walker GC, Blanco C. 2010. Proteomic alterations explain phenotypic changes in *Sinorhizobium meliloti* lacking the RNA chaperone Hfq. *J Bacteriol* **192**: 1719–1729.

Bartel J, Varadarajan AR, Sura T, Ahrens CH, Maaß S, Becher D. 2020. Optimized proteomics workflow for the detection of small proteins. *J Proteome Res* **19**: 4004–4018.

Bartholomäus A, Del Campo C, Ignatova Z. 2016. Mapping the non-standardized biases of ribosome profiling. *Biol Chem* **397**: 23–35.

Baumgartner D, Kopf M, Klähn S, Steglich C, Hess WR. 2016. Small proteins in cyanobacteria provide a paradigm for the functional analysis of the bacterial micro-proteome. *BMC Microbiol* **16**: 285.

Becker A, Bergès H, Krol E, Bruand C, Rüberg S, Capela D, Lauber E, Meilhoc E, Ampe F, de Bruijn FJ, et al. 2004. Global changes in gene expression in *Sinorhizobium meliloti* 1021 under microoxic and symbiotic conditions. *Mol Plant Microbe Interact* **17**: 292–303.

Becker AH, Oh E, Weissman JS, Kramer G, Bukau B. 2013. Selective ribosome profiling as a tool for studying the interaction of chaperones and targeting factors with nascent polypeptide chains and ribosomes. *Nat Protoc* **8**: 2212–2239.

Beringer JE. 1974. R factor transfer in *Rhizobium leguminosarum*. *J Gen Microbiol* **84**: 188–198.

Blakeley P, Overton IM, Hubbard SJ. 2012. Addressing statistical biases in nucleotide-derived protein databases for proteogenomic search strategies. *J Proteome Res* **11**: 5221–5234.

Buels R, Yao E, Diesh CM, Hayes RD, Munoz-Torres M, Helt G, Goodstein DM, Elsik CG, Lewis SE, Stein L, et al. 2016. JBrowse: a dynamic web platform for genome visualization and analysis. *Genome Biol* **17**: 66.

Burger T. 2018. Gentle introduction to the statistical foundations of false discovery rate in quantitative proteomics. *J Proteome Res* **17**: 12–22.

Casse F, Boucher C, Julliot JS, Michel M, Denarie J. 1979. Identification and Characterization of Large Plasmids in *Rhizobium meliloti* using Agarose Gel Electrophoresis. *J Gen Microbiol* **113**: 229–242.

Cassidy L, Kaulich PT, Maaß S, Bartel J, Becher D, Tholey A. 2021. Bottom-up and top-down proteomic approaches for the identification, characterization and quantification of the low molecular weight proteome with focus on short open reading frame-encoded peptides. *Proteomics* e2100008.

1   Cassidy L, Kaulich PT, Tholey A. 2019. Depletion of High-Molecular-Mass Proteins for the
2   Identification of Small Proteins and Short Open Reading Frame Encoded Peptides in
3   Cellular Proteomes. *J Proteome Res* **18**: 1725–1734.

4   Charoenpanich P, Meyer S, Becker A, McIntosh M. 2013. Temporal expression program of
5   quorum sensing-based transcription regulation in *Sinorhizobium meliloti. J Bacteriol*
6   **195**: 3224–3236.

7   Cianciulli Sesso A, Lilić B, Amman F, Wolfinger MT, Sonnleitner E, Bläsi U. 2021. Gene
8   Expression Profiling of *Pseudomonas aeruginosa* Upon Exposure to Colistin and
9   Tobramycin. *Front Microbiol* **12**: 626715.

10 Clauwaert J, Menschaert G, Waegeman W. 2019. DeepRibo: a neural network for precise
11   gene annotation of prokaryotes by combining ribosome profiling signal and binding
12   site patterns. *Nucleic Acids Res* **47**: e36.

13 Čuklina J, Hahn J, Imakaev M, Omasits U, Förstner KU, Ljubimov N, Goebel M, Pessi G,
14   Fischer H-M, Ahrens CH, et al. 2016. Genome-wide transcription start site mapping of
15   *Bradyrhizobium japonicum* grown free-living or in symbiosis - a rich resource to
16   identify new transcripts, proteins and to study gene regulation. *BMC Genomics* **17**: 302.

17 Djordjevic MA. 2004. *Sinorhizobium meliloti* metabolism in the root nodule: a proteomic
18   perspective. *Proteomics* **4**: 1859–1872.

19 Dodbele S, Wilusz JE. 2020. Ending on a high note: Downstream ORFs enhance mRNA
20   translational output. *EMBO J* **39**: e105959.

21 Duval M, Cossart P. 2017. Small bacterial and phagic proteins: an updated view on a
22   rapidly moving field. *Curr Opin Microbiol* **39**: 81–88.

23 Evguenieva-Hackenberg E. 2022. Riboregulation in bacteria: From general principles to
24   novel mechanisms of the *trp* attenuator and its sRNA and peptide products. *Wiley*
25   *Interdiscip Rev RNA* **13**: e1696.

26 Ewels P, Magnusson M, Lundin S, Käller M. 2016. MultiQC: summarize analysis results for
27   multiple tools and samples in a single report. *Bioinformatics* **32**: 3047–3048.

28 Fancello L, Burger T. 2022. An analysis of proteogenomics and how and when
29   transcriptome-informed reduction of protein databases can enhance eukaryotic
30   proteomics. *Genome Biol* **23**: 132.

31 Fijalkowski I, Willems P, Jonckheere V, Simoens L, Van Damme P. 2022. Hidden in plain
32   sight: challenges in proteomics detection of small ORF-encoded polypeptides. *microLife*
33   **3**.

34 Galibert F, Finan TM, Long SR, Puhler A, Abola P, Ampe F, Barloy-Hubler F, Barnett MJ,
35   Becker A, Boistard P, et al. 2001. The composite genome of the legume symbiont
36   *Sinorhizobium meliloti*. *Science* **293**: 668–672.

37 Gelhausen R, Müller T, Svensson SL, Alkhnbashi OS, Sharma CM, Eggenhofer F, Backofen
38   R. 2022. RiboReport - benchmarking tools for ribosome profiling-based identification
39   of open reading frames in bacteria. *Brief Bioinformatics* **23**.

40 Gelhausen R, Svensson SL, Froschauer K, Heyl F, Hadjeras L, Sharma CM, Eggenhofer F,
41   Backofen R. 2021. HRIBO: high-throughput analysis of bacterial ribosome profiling
42   data. *Bioinformatics* **37**: 2061–2063.

1   Gelsinger DR, Dallon E, Reddy R, Mohammad F, Buskirk AR, DiRuggiero J. 2020. Ribosome
2   profiling in archaea reveals leaderless translation, novel translational initiation sites,
3   and ribosome pausing at single codon resolution. *Nucleic Acids Res* **48**: 5201–5216.

4   Gerashchenko MV, Gladyshev VN. 2014. Translation inhibitors cause abnormalities in
5   ribosome profiling experiments. *Nucleic Acids Res* **42**: e134.

6   Gertz EM, Yu Y-K, Agarwala R, Schäffer AA, Altschul SF. 2006. Composition-based statistics
7   and translated nucleotide searches: improving the TBLASTN module of BLAST. *BMC*
8   *Biol* **4**: 41.

9   Glaub A, Huptas C, Neuhaus K, Ardern Z. 2020. Recommendations for bacterial ribosome
10   profiling experiments based on bioinformatic evaluation of published data. *J Biol Chem*
11   **295**: 8999–9011.

12 Gray T, Storz G, Papenfort K. 2022. Small proteins; big questions. *J Bacteriol* **204**:
13   e0034121.

14 Grüning B, Dale R, Sjödin A, Chapman BA, Rowe J, Tomkins-Tinch CH, Valieris R, Köster J,
15   Bioconda Team. 2018. Bioconda: sustainable and comprehensive software distribution
16   for the life sciences. *Nat Methods* **15**: 475–476.

17 Grützner J, Billenkamp F, Spanka D-T, Rick T, Monzon V, Förstner KU, Klug G. 2021. The
18   small DUF1127 protein CcaF1 from *Rhodobacter sphaeroides* is an RNA-binding protein
19   involved in sRNA maturation and RNA turnover. *Nucleic Acids Res* **49**: 3003–3019.

20 Guan Y, Zhu Q, Huang D, Zhao S, Jan Lo L, Peng J. 2015. An equation to estimate the
21   difference between theoretically predicted and SDS PAGE-displayed molecular weights
22   for an acidic peptide. *Sci Rep* **5**: 13370.

23 Hahn J, Tsoy OV, Thalmann S, Čuklina J, Gelfand MS, Evguenieva-Hackenberg E. 2016.
24   Small Open Reading Frames, Non-Coding RNAs and Repetitive Elements in
25   *Bradyrhizobium japonicum* USDA 110. *PLoS ONE* **11**: e0165429.

26 Hemm MR, Weaver J, Storz G. 2020. Escherichia coli Small Proteome. *Ecosal Plus* **9**.

27 Ingolia NT, Brar GA, Rouskin S, McGeachy AM, Weissman JS. 2012. The ribosome profiling
28   strategy for monitoring translation in vivo by deep sequencing of ribosome-protected
29   mRNA fragments. *Nat Protoc* **7**: 1534–1550.

30 Ingolia NT, Ghaemmaghami S, Newman JRS, Weissman JS. 2009. Genome-wide analysis in
31   vivo of translation with nucleotide resolution using ribosome profiling. *Science* **324**:
32   218–223.

33 Ingolia NT, Hussmann JA, Weissman JS. 2019. Ribosome profiling: global views of
34   translation. *Cold Spring Harb Perspect Biol* **11**.

35 Ingolia NT. 2016. Ribosome Footprint Profiling of Translation throughout the Genome.
36   *Cell* **165**: 22–33.

37 Jones KM, Kobayashi H, Davies BW, Taga ME, Walker GC. 2007. How rhizobial symbionts
38   invade plants: the *Sinorhizobium-Medicago* model. *Nat Rev Microbiol* **5**: 619–633.

39 Karzai AW, Roche ED, Sauer RT. 2000. The SsrA-SmpB system for protein tagging, directed
40   degradation and ribosome rescue. *Nat Struct Biol* **7**: 449–455.

41 Kaulich PT, Cassidy L, Bartel J, Schmitz RA, Tholey A. 2021. Multi-protease Approach for
42   the Improved Identification and Molecular Characterization of Small Proteins and
43   Short Open Reading Frame-Encoded Peptides. *J Proteome Res* **20**: 2895–2903.

Keiler KC, Shapiro L, Williams KP. 2000. tmRNAs that encode proteolysis-inducing tags are found in all known bacterial genomes: A two-piece tmRNA functions in *Caulobacter*. *Proc Natl Acad Sci USA* **97**: 7778–7783.

Kelley LA, Mezulis S, Yates CM, Wass MN, Sternberg MJE. 2015. The Phyre2 web portal for protein modeling, prediction and analysis. *Nat Protoc* **10**: 845–858.

Khan SR, Gaines J, Roop RM, Farrand SK. 2008. Broad-host-range expression vectors with tightly regulated promoters and their use to examine the influence of TraR and TraM expression on Ti plasmid quorum sensing. *Appl Environ Microbiol* **74**: 5053–5062.

Khitun A, Slavoff SA. 2019. Proteomic detection and validation of translated small open reading frames. *Curr Protoc Chem Biol* **11**: e77.

Knoke LR, Abad Herrera S, Götz K, Justesen BH, Günther Pomorski T, Fritz C, Schäkermann S, Bandow JE, Aktas M. 2020. *Agrobacterium tumefaciens* Small Lipoprotein Atu8019 Is Involved in Selective Outer Membrane Vesicle (OMV) Docking to Bacterial Cells. *Front Microbiol* **11**: 1228.

Köster J, Rahmann S. 2012. Snakemake--a scalable bioinformatics workflow engine. *Bioinformatics* **28**: 2520–2522.

Kovacs-Simon A, Titball RW, Michell SL. 2011. Lipoproteins of bacterial pathogens. *Infect Immun* **79**: 548–561.

Kraus A, Weskamp M, Zierles J, Balzer M, Busch R, Eisfeld J, Lambertz J, Nowaczyk MM, Narberhaus F. 2020. Arginine-Rich Small Proteins with a Domain of Unknown Function, DUF1127, Play a Role in Phosphate and Carbon Metabolism of *Agrobacterium tumefaciens*. *J Bacteriol* **202**.

Krogh A, Larsson B, von Heijne G, Sonnhammer ELL. 2001. Predicting transmembrane protein topology with a hidden Markov model: application to complete genomes. *J Mol Biol* **305**: 567–580.

Liao Y, Smyth GK, Shi W. 2014. featureCounts: an efficient general purpose program for assigning sequence reads to genomic features. *Bioinformatics* **30**: 923–930.

Li H, Handsaker B, Wysoker A, Fennell T, Ruan J, Homer N, Marth G, Abecasis G, Durbin R, 1000 Genome Project Data Processing Subgroup. 2009. The Sequence Alignment/Map format and SAMtools. *Bioinformatics* **25**: 2078–2079.

Li H, Joh YS, Kim H, Paek E, Lee S-W, Hwang K-B. 2016. Evaluating the effect of database inflation in proteogenomic search on sensitive and reliable peptide identification. *BMC Genomics* **17**: 1031.

Marlow VL, Haag AF, Kobayashi H, Fletcher V, Scocchi M, Walker GC, Ferguson GP. 2009. Essential role for the BacA protein in the uptake of a truncated eukaryotic peptide in *Sinorhizobium meliloti*. *J Bacteriol* **191**: 1519–1527.

Martin M. 2011. Cutadapt removes adapter sequences from high-throughput sequencing reads. *EMBnet j* **17**: 10.

Marx H, Minogue CE, Jayaraman D, Richards AL, Kwiecien NW, Siahpirani AF, Rajasekar S, Maeda J, Garcia K, Del Valle-Echevarria AR, et al. 2016. A proteomic atlas of the legume Medicago truncatula and its nitrogen-fixing endosymbiont *Sinorhizobium meliloti*. *Nat Biotechnol* **34**: 1198–1205.

McIntosh M, Krol E, Becker A. 2008. Competitive and cooperative effects in quorum-sensing-regulated galactoglucan biosynthesis in *Sinorhizobium meliloti*. *J Bacteriol* **190**: 5308–5317.

Melior H, Li S, Madhugiri R, Stötzel M, Azarderakhsh S, Barth-Weber S, Baumgardt K, Ziebuhr J, Evguenieva-Hackenberg E. 2019. Transcription attenuation-derived small RNA rnTrpL regulates tryptophan biosynthesis gene expression in trans. *Nucleic Acids Res* **47**: 6396–6410.

Melior H, Li S, Stötzel M, Maaß S, Schütz R, Azarderakhsh S, Shevkoplias A, Barth-Weber S, Baumgardt K, Ziebuhr J, et al. 2021. Reprograming of sRNA target specificity by the leader peptide peTrpL in response to antibiotic exposure. *Nucleic Acids Res* **49**: 2894–2915.

Melior H, Maaß S, Li S, Förstner KU, Azarderakhsh S, Varadarajan AR, Stötzel M, Elhossary M, Barth-Weber S, Ahrens CH, et al. 2020. The Leader Peptide peTrpL Forms Antibiotic-Containing Ribonucleoprotein Complexes for Posttranscriptional Regulation of Multiresistance Genes. *MBio* **11**.

Meydan S, Marks J, Klepacki D, Sharma V, Baranov PV, Firth AE, Margus T, Kefi A, Vázquez-Laslop N, Mankin AS. 2019. Retapamulin-Assisted Ribosome Profiling Reveals the Alternative Bacterial Proteome. *Mol Cell* **74**: 481-493.e6.

Mohammad F, Green R, Buskirk AR. 2019. A systematically-revised ribosome profiling method for bacteria reveals pauses at single-codon resolution. *eLife* **8**.

Ndah E, Jonckheere V, Giess A, Valen E, Menschaert G, Van Damme P. 2017. REPARATION: ribosome profiling assisted (re-)annotation of bacterial genomes. *Nucleic Acids Res* **45**: e168.

Nesvizhskii AI. 2010. A survey of computational methods and error rate estimation procedures for peptide and protein identification in shotgun proteomics. *J Proteomics* **73**: 2092–2123.

Oh E, Becker AH, Sandikci A, Huber D, Chaba R, Gloge F, Nichols RJ, Typas A, Gross CA, Kramer G, et al. 2011. Selective ribosome profiling reveals the cotranslational chaperone action of trigger factor in vivo. *Cell* **147**: 1295–1308.

Omasits U, Quebatte M, Stekhoven DJ, Fortes C, Roschitzki B, Robinson MD, Dehio C, Ahrens CH. 2013. Directed shotgun proteomics guided by saturated RNA-seq identifies a complete expressed prokaryotic proteome. *Genome Res* **23**: 1916–1927.

Omasits U, Varadarajan AR, Schmid M, Goetze S, Melidis D, Bourqui M, Nikolayeva O, Québatte M, Patrignani A, Dehio C, et al. 2017. An integrative strategy to identify the entire protein coding potential of prokaryotic genomes by proteogenomics. *Genome Res* **27**: 2083–2095.

Orr MW, Mao Y, Storz G, Qian S-B. 2020. Alternative ORFs and small ORFs: shedding light on the dark proteome. *Nucleic Acids Res* **48**: 1029–1042.

Otto C, Stadler PF, Hoffmann S. 2014. Lacking alignments? The next-generation sequencing mapper segemehl revisited. *Bioinformatics* **30**: 1837–1843.

Patraquim P, Mumtaz MAS, Pueyo JI, Aspden JL, Couso J-P. 2020. Developmental regulation of canonical and small ORF translation from mRNAs. *Genome Biol* **21**: 128.

1 Petruschke H, Anders J, Stadler PF, Jehmlich N, von Bergen M. 2020. Enrichment and identification of small proteins in a simplified human gut microbiome. *J Proteomics* **213**: 103604.

Petruschke H, Schori C, Canzler S, Riesbeck S, Poehlein A, Daniel R, Frei D, Segessemann T, Zimmerman J, Marinos G, et al. 2021. Discovery of novel community-relevant small proteins in a simplified human intestinal microbiome. *Microbiome* **9**: 55.

Qeli E, Ahrens CH. 2010. PeptideClassifier for protein inference and targeted quantitative proteomics. *Nat Biotechnol* **28**: 647–650.

Sallet E, Roux B, Sauviac L, Jardinaud M-F, Carrère S, Faraut T, de Carvalho-Niebel F, Gouzy J, Gamas P, Capela D, et al. 2013. Next-generation annotation of prokaryotic genomes with EuGene-P: application to *Sinorhizobium meliloti* 2011. *DNA Res* **20**: 339–354.

Schägger H. 2006. Tricine-SDS-PAGE. *Nat Protoc* **1**: 16–22.

Schlüter J-P, Reinkensmeier J, Barnett MJ, Lang C, Krol E, Giegerich R, Long SR, Becker A. 2013. Global mapping of transcription start sites and promoter motifs in the symbiotic α-proteobacterium *Sinorhizobium meliloti* 1021. *BMC Genomics* **14**: 156.

Sharma CM, Darfeuille F, Plantinga TH, Vogel J. 2007. A small RNA regulates multiple ABC transporter mRNAs by targeting C/A-rich elements inside and upstream of ribosome-binding sites. *Genes Dev* **21**: 2804–2817.

Simon R, Priefer U, Pühler A. 1983. A broad host range mobilization system for *in vivo* genetic engineering: transposon mutagenesis in gram negative bacteria. *Nat Biotechnol* **1**: 784–791.

Sobrero P, Schlüter J-P, Lanner U, Schlosser A, Becker A, Valverde C. 2012. Quantitative proteomic analysis of the Hfq-regulon in *Sinorhizobium meliloti* 2011. *PLoS ONE* **7**: e48494.

Song K, Baumgartner D, Hagemann M, Muro-Pastor AM, Maaß S, Becher D, Hess WR. 2022. AtpΘ is an inhibitor of F0F1 ATP synthase to arrest ATP hydrolysis during low-energy conditions in cyanobacteria. *Curr Biol* **32**: 136-148.e5.

Stekhoven DJ, Omasits U, Quebatte M, Dehio C, Ahrens CH. 2014. Proteome-wide identification of predominant subcellular protein localizations in a bacterial model organism. *J Proteomics* **99**: 123–137.

Storz G, Wolf YI, Ramamurthi KS. 2014. Small proteins can no longer be ignored. *Annu Rev Biochem* **83**: 753–777.

Sun Y-H, de Jong MF, den Hartigh AB, Roux CM, Rolán HG, Tsolis RM. 2012. The small protein CydX is required for function of cytochrome bd oxidase in *Brucella abortus*. *Front Cell Infect Microbiol* **2**: 47.

Torres-Quesada O, Millán V, Nisa-Martínez R, Bardou F, Crespi M, Toro N, Jiménez-Zurdo JI. 2013. Independent activity of the homologous small regulatory RNAs AbcR1 and AbcR2 in the legume symbiont *Sinorhizobium meliloti*. *PLoS ONE* **8**: e68147.

Tyanova S, Temu T, Cox J. 2016. The MaxQuant computational platform for mass spectrometry-based shotgun proteomics. *Nat Protoc* **11**: 2301–2319.

Ulvé VM, Chéron A, Trautwetter A, Fontenelle C, Barloy-Hubler F. 2007. Characterization and expression patterns of *Sinorhizobium meliloti* tmRNA (ssrA). *FEMS Microbiol Lett* **269**: 117–123.

1 VanOrsdel CE, Kelly JP, Burke BN, Lein CD, Oufiero CE, Sanchez JF, Wimmers LE, Hearn DJ,
2 Abuikhdair FJ, Barnhart KR, et al. 2018. Identifying New Small Proteins in *Escherichia*
3 *coli*. *Proteomics* **18**: e1700064.

4 Varadarajan AR, Allan RN, Valentin JDP, Castañeda Ocampo OE, Somerville V, Pietsch F,
5 Buhmann MT, West J, Skipp PJ, van der Mei HC, et al. 2020a. An integrated model
6 system to gain mechanistic insights into biofilm-associated antimicrobial resistance in
7 *Pseudomonas aeruginosa* MPAO1. *npj Biofilms and Microbiomes* **6**: 46.

8 Varadarajan AR, Goetze S, Pavlou MP, Grosboillot V, Shen Y, Loessner MJ, Ahrens CH,
9 Wollscheid B. 2020b. A Proteogenomic Resource Enabling Integrated Analysis of
10 *Listeria* Genotype-Proteotype-Phenotype Relationships. *J Proteome Res* **19**: 1647–
11 1662.

12 Vazquez-Laslop N, Sharma CM, Mankin A, Buskirk AR. 2022. Identifying Small Open
13 Reading Frames in Prokaryotes with Ribosome Profiling. *J Bacteriol* **204**: e0029421.

14 Venturini E, Svensson SL, Maaß S, Gelhausen R, Eggenhofer F, Li L, Cain AK, Parkhill J,
15 Becher D, Backofen R, et al. 2020. A global data-driven census of *Salmonella* small
16 proteins and their potential functions in bacterial virulence. *microLife*. doi:
17 10.1093/femsml/uqaa002.

18 Vitreschak AG, Lyubetskaya EV, Shirshin MA, Gelfand MS, Lyubetsky VA. 2004.
19 Attenuation regulation of amino acid biosynthetic operons in proteobacteria:
20 comparative genomics analysis. *FEMS Microbiol Lett* **234**: 357–370.

21 Weaver J, Mohammad F, Buskirk AR, Storz G. 2019. Identifying Small Proteins by
22 Ribosome Profiling with Stalled Initiation Complexes. *MBio* **10**.

23 Wingett SW, Andrews S. 2018. FastQ Screen: A tool for multi-genome mapping and quality
24 control. [version 2; peer review: 4 approved]. *F1000Res* **7**: 1338.

25 Wiśniewski JR. 2016. Quantitative evaluation of filter aided sample preparation (FASP)
26 and multienzyme digestion FASP protocols. *Anal Chem* **88**: 5438–5443.

27 Wu Q, Wright M, Gogol MM, Bradford WD, Zhang N, Bazzini AA. 2020. Translation of small
28 downstream ORFs enhances translation of canonical main open reading frames. *EMBO*
29 *J* **39**: e104763.

30 Yu NY, Wagner JR, Laird MR, Melli G, Rey S, Lo R, Dao P, Sahinalp SC, Ester M, Foster LJ, et
31 al. 2010. PSORTb 3.0: improved protein subcellular localization prediction with refined
32 localization subcategories and predictive capabilities for all prokaryotes.
33 *Bioinformatics* **26**: 1608–1615.

34 Zeghouf M, Li J, Butland G, Borkowska A, Canadien V, Richards D, Beattie B, Emili A,
35 Greenblatt JF. 2004. Sequential Peptide Affinity (SPA) system for the identification of
36 mammalian and bacterial protein complexes. *J Proteome Res* **3**: 463–468.

37 Zevenhuizen LPTM, van Neerven ARW. 1983. (1→2)-β-d-glucan and acidic
38 oligosaccharides produced by *Rhizobium meliloti*. *Carbohydr Res* **118**: 127–134.

39 Zhang Y, Fonslow BR, Shan B, Baek M-C, Yates JR. 2013. Protein analysis by
40 shotgun/bottom-up proteomics. *Chem Rev* **113**: 2343–2394.

41

42

List of Supplementary Figures and Supplementary Tables

Figure S1. Schematic representation of the plasmids used in this study. pRS1: The plasmid that was used as a vector backbone (the multiple cloning site [MCS] is shown) to create the following plasmids (all shown below): pRS1-T$_{rrn}$: RS1 derivative with cloned transcriptional terminator (T$_{rrn}$). pSW1: pRS1-T$_{rrn}$ derivative with cloned sequence of the SPA-tag (SPA), preceded by a linker (L). pSW2: pSW1 derivative with cloned promoter P$_{sinI}$, which is constitutively active in *Sinorhizobium meliloti* 2011 during growth. pSW2-SEP: pSW2 derivative with a cloned sORF and its −15 5′ UTR region potentially harboring a Shine-Dalgarno sequence; the sORF is cloned without the stop codon in frame with the linker and the SPA tag.

Figure S2. Metagene analysis of *Sinorhizobium meliloti* ribosome footprints. Genome-wide analysis of ribosome occupancy near annotated start codons. The recovered ribosome footprints (length distribution varies from 27 nt to 33 nt) were mapped using **(A)** 5′ end and **(B)** 3′ end approaches. Metagene analysis of the 32-nt-long ribosome footprints by the 5′ end **(C)** and 3′ end **(D)** mapping approaches shows that the ribosome protects a region of 16 nt upstream and downstream of annotated start codons (+1; first nucleotide of the start codon).

Figure S3. Examples of genomic regions with high translation efficiency (TE). (A) The *gabD1* gene (SM2011_c02780) encoding for succinate semialdehyde dehydrogenase harbors a short 5′ UTR (24 nt), which exhibits ribosome protection at −15/−16 upstream of the start codon that contributes to its high TE value (TE = 34.6). **(B)** The 3′ UTR of the SM2011_c01202 gene encoding lipoprotein shows high ribosome density and TE. HRIBO predicts a potential novel downstream small open reading frame (sORF) in this region (25 amino acids [aa], TE = 4.3). **(C)** A novel sORF is predicted in the non-coding small RNA (sRNA) SMc06505 (38 aa, TE = 3.23). This can be an example of dual-function sRNA in *Sinorhizobium meliloti* 2011. Genomic locations and coding regions are indicated below the image. Bent arrows indicate the transcription start sites based on (Sallet et al. 2013).

48

1 **Figure S4. Comparison of search results against the standard and custom-**
2 **integrated proteogenomic search databases (iPtgxDBs). (A)** Venn diagram with an
3 overview of the proteins identified by the three different experimental approaches (the
4 colors match those from Figure 5A: gray, green, and blue represent the trypsin digest, SPE
5 and Lys-C digest, and SPE and no protease digestion, respectively). **(B)** The Venn diagram
6 shows the overlap of the number of proteins identified in the searches against the two
7 iPtgxDBs (standard and custom iPtgxDB). The search against the 20-fold smaller custom
8 iPtgxDb allowed the identification of 112 proteins that were not identified in the search
9 against the much larger standard iPtgxDB. These hits include RefSeq or GenBank
10 annotations. The 18 unique identifications made with the standard iPtgxDB include novel
11 proteins or proteoforms contributed from Chemgenome *ab initio* predictions or *in silico*
12 predictions that are not contained in the small custom iPtgxDB.

13

14 **Figure S5. Mass spectrometry of selected novel small open reading frame-encoded**
15 **proteins (SEPs).** Here, we show some of the spectra that allowed us to identify novel
16 SEPs. If more than one peptide spectrum match (PSM) was detected for a given peptide
17 ion, a representative spectrum was selected. MS2 spectra with assigned fragment ion m/z
18 (left) and fragmentation tables (right) were obtained with Scaffold V4.8.7 using the search
19 output files (*.sf3), which were deposited at the ProteomeXchange Consortium with the
20 dataset identifier PXD034931. Colored m/z were assigned in the identifying MS2 spectra.

21

22 **Figure S6. Analysis of a putative small open reading frame (sORF) in tmRNA of**
23 ***Sinorhizobium meliloti* 2011. (A)** Schematic view of the chromosomal *ssrA* locus
24 corresponding to tmRNA, which is discontinuous in Alphaproteobacteria due to post-
25 transcriptional removal of the indicated internal segment (Keiler et al. 2000; Ulvé et al.
26 2007). The tRNA and mRNA parts of the tmRNA and their lengths are indicated. In the
27 mRNA part, a putative sORF corresponding to a 23-amino acid (aa) SEP was predicted
28 (the potential SEP sequence is shown). The 3′ part of the sORF corresponds to the
29 proteolytic tag-encoding sequence (the alanine encoded by the resume codon is shown in
30 bold). The indicated parts of the *ssrA* gene were cloned in pSW2, and the *S. meliloti* 2011
31 strains containing the corresponding plasmids were used for Western blot analysis. While

1   no specific bands were detected in lysates of the pSW2-ssrA1-containing plasmid, which

2   lacks the tRNA part of tmRNA (data not shown), a strong signal was obtained with the

3   pSW2-ssrA2 plasmid, which contains both the tRNA and mRNA parts (see panel C). **(B)**

4   Schematic representation of the *ssrA* part cloned in pSW2-ssrA2. The used mutations are

5   indicated. 1: Conserved GG nucleotides upstream of the putative start codon TTG were

6   mutated to TT. 2: The resume codon was changed to encode valine instead of alanine. 3:

7   The putative start codon TTG was mutated to the stop codon TAG. **(C)** Western blot

8   analysis with antibodies directed against the FLAG part of the sequential peptide affinity

9   (SPA) tag, which was fused in frame to the proteolytic tag. Crude lysates (corresponding

10   to 20 OD) of *S. meliloti* 2011 strains containing the indicated plasmids (see panels A and

11   B) were analyzed. The detected bands above 25 kDA have identical lengths. Expression of

12   the corresponding SPA-tagged peptide was abolished by the indicated GG/TT mutation,

13   which disrupts conserved base pairing in the tmRNA (Keiler et al. 2000), whereas a weak

14   signal was still detected when the resume codon was mutated. Destroying the putative 23

15   aa sORF (TTG/TAG mutation in variant 3) did not abolish the expression of the tagged

16   peptide. These results, combined with no detection of a peptide using pSW2-ssrA1,

17   suggest that the SPA-tagged peptide detected in panel C corresponds to the 12 aa

18   proteolytic tag and not to the putative 23 aa SEP. Furthermore, the data support the

19   important role of the analyzed GG nucleotides for the tmRNA function.

20

21   **Figure S7. Analysis of the S100 and P100 fractions of *Sinorhizobium meliloti* 2011**

22   **strains producing the indicated small open reading frame-encoded proteins (SEPs)**

23   **from pSW2-SEP plasmids.** The empty vector control (EVC) strain was used as the

24   negative control. Identical volumes of the S100 and P100 fractions were loaded. Top

25   panels: Western blot analysis with monoclonal anti-FLAG antibodies. Bottom panels:

26   Coomassie-stained gels, in which the used protein fractions are shown. Migration of

27   marker proteins (in kDa) is shown on the left side, and exposition times are indicated. *

28   Unspecific signal.

29

30

31

Supplementary Tables

Table S1. Distribution of total mapped reads to different annotated RNA classes.

The table indicates the total number of mapped reads mapping to annotations for different RNA classes (mRNA, rRNA, and tRNA).

Table S2. Translation efficiency values for all annotated genes of *Sinorhizobium meliloti* 2011.

This table is generated by the HRIBO pipeline and contains information about the annotated features extracted from the used GenBank 2014 annotation. It contains information, such as the gene identifier, the start and stop codons, the encoding strand, locus tags, nucleotides/amino acid sequences, and information regarding the encoded protein, translation efficiency (TE), as well as the RPKM values. The RPKM values were calculated directly after the removal of multi-mapping reads and before the removal of reads mapping to rRNA.

Table S3. Overview of the six integrated proteogenomic search databases (iPtgxDBs) created for this project.

Three large standard iPtgxDBs were created: one for trypsin, one for Lys-C, and a modified version for the experimental approach without proteolytic digestion. On the top, three approximately 20-fold smaller custom iPtgxDBs were created using experimental ribosome profiling data instead of the Chemgenome *ab initio* predictions and the large number of *in silico* predictions that aim to capture the entire protein coding potential.

Table S3.1: Size of the six annotation sources (three reference genome annotations, two *ab initio* predictions, and the *in silico* prediction) and the added novelty (new clusters, new reductions, and new extensions) achieved through the step-wise, hierarchical integration carried out for the standard iPtgxDBs.

Table S3.2: Database entries and number of excluded entries for the three standard iPtgxDBs for trypsin, Lys-C, and without proteolytic digestion.

1   **Table S3.3:** Size of the five annotation sources (three reference genome annotations, one

2   *ab initio* prediction, and experimental ribosome profiling data) and the added novelty

3   (new clusters, new reductions, new extensions) achieved through the step-wise,

4   hierarchical integration carried out for the three smaller custom iPtgxDBs.

5   **Table S3.4:** Database entries and number of excluded entries for the three custom

6   iPtgxDBs for trypsin, LysC, and without proteolytic digestion.

7

8   **Table S4. "Master table", with an overview of various datasets detailed in the**

9   **manuscript.**

10   This table lists several datasets described in the manuscript and allows researchers to

11   select/filter them. It contains information about genomic location and annotation for the

12   6263 CDS (GenBank 2014 annotation) and their match with the RefSeq 2017 annotation.

13   For the ribosome profiling (Ribo-seq) data, we listed the 3,758 GenBank annotated open

14   reading frames (ORFs) identified as translated in minimal medium (translation efficiency

15   [TE] of ≥ 0.5 and RNA-seq and Ribo-seq RPKM of ≥ 10), all 259 GenBank annotated small

16   (sORFs) (≤ 70 amino acids [aa]), and the 85 GenBank annotated sORFs identified as

17   translated after manual curation (Figures 2 and 3). Furthermore, listed are the 266

18   potentially novel Ribo-seq implied sORFs (not present in the GenBank 2014 annotation;

19   TE of ≥ 0.5, RNA-seq and Ribo-seq RPKM of ≥ 10, DeepRibo score of > −0.5), and the subset

20   of 54 manually curated, high-confidence non-annotated sORFs (Figure 4). For the mass

21   spectrometry (MS) data, a list of 191 sORF-encoded proteins (SEPs) can be filtered, among

22   which at least one peptide spectrum match (PSM) was identified, the 58 SEPs that pass

23   the more stringent PSM filters (Figure 5), and the respective search database results

24   where they were detected (standard integrated proteogenomic search databases

25   [iPtgxDB], custom iPtgxDB or both). A total of 20 candidates for which Western blot

26   validation was attempted (15 thereof with success) can then be selected (Figure 6), as

27   well as the 48 novel sORFs missing from both the GenBank 2014 and Refseq 2017

28   annotations, and 37 detected by Ribo-seq and 11 by proteomics (Figure 7). Finally, the

29   PSM counts and identifiers contained in the large standard iPtgxDB and the small custom

30   iPtgxDB of the 1,219 proteins identified by MS are provided.

31

Table S5. Oligonucleotides used in this study.

Table S6. List of annotated open reading frames (ORFs) and small ORFs (sORFs) detected as translated in *Sinorhizobium meliloti* 2011 by ribosome profiling (Ribo-seq).

Using Ribo-seq (average translation efficiency [TE] of ≥ 0.5 and RNA-seq and Ribo-seq RPKM of ≥ 10 in both replicates), translation was detected for 3,758 ORFs out of the 6,263 annotated ORFs. In addition, we manually curated each annotated sORF with an average TE of ≥ 0.5 and RNA-seq and Ribo-seq RPKM of ≥ 10 (in both replicates) in a genome browser. Based on the manual curation, translation was detected for 85 of the 259 annotated *Sinorhizobium meliloti* sORFs (GenBank annotation 2014).

Table S7: List of non-annotated translated small open reading frames (sORFs) identified in *Sinorhizobium meliloti* 2011 by ribosome profiling (Ribo-seq).

The two prediction tools DeepRibo and Reparation, which are implemented in the HRIBO pipeline, predicted a high number of translated sORFs (approximately 15,000 sORFs). To cope with and prioritize this high number of predictions, we first applied cut-offs (average translation efficiency of ≥ 0.5 and RNA-seq and Ribo-seq RPKM of ≥ 10 in both replicates, and DeepRibo score of > −0.5), which resulted in a list of 266 potential, translated, non-annotated sORFs (see Table S4) (GenBank annotation 2014). We then manually curated each of these 266 predicted sORFs in a genome browser. The resulting list of 54 non-annotated sORFs, which we propose with high confidence to be translated, is presented in this table..

Table S8: List of the 48 novel small open reading frames identified in *Sinorhizobium meliloti* 2011 using ribosome profiling and proteomics. A list of Phyre2 best hits is also provided.